

**UCSF**

**UC San Francisco Electronic Theses and Dissertations**

**Title**

Development of a CRISPR activation-based approach for the treatment of SCN2A haploinsufficiency in Autism Spectrum Disorder

**Permalink**

<https://escholarship.org/uc/item/55d6b9cm>

**Author**

Tamura, Serena

**Publication Date**

2021

Peer reviewed|Thesis/dissertation

Development of a CRISPR activation-based approach for the treatment of SCN2A haploinsufficiency in Autism Spectrum Disorder

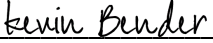
by  
Serena Tamura

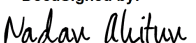
DISSERTATION  
Submitted in partial satisfaction of the requirements for degree of  
DOCTOR OF PHILOSOPHY

in  
Pharmaceutical Sciences and Pharmacogenomics


in the  
GRADUATE DIVISION  
of the  
UNIVERSITY OF CALIFORNIA, SAN FRANCISCO

Approved:

DocuSigned by:  
  
A996F2A5C1214BE... Kevin Bender  
Chair

DocuSigned by:  
  
Nadav Ahituv

DocuSigned by:  
  
Stephan Sanders

DocuSigned by:  
  
613938B56C88470... Georgia Panagiotakos

---

Committee Members



## **Dedication and Acknowledgements**

I would like to dedicate this dissertation to my late grandmother Setsuko Tanaka. She enveloped me with her love of reading, learning, flowers and cream puffs from a young age and I carry her joy with me always.

First, I would like to thank my mentor and professor Dr. Nadav Ahituv for providing me with incredible support and guidance over the last six years. I never dreamed of working on a project so close to my personal quest of developing precision therapies in currently untreatable disorders and you not only gave me this opportunity, but also guided me with understanding, patience and unwavering support. Thank you for shaping me as a scientist and researcher with the strength and tenacity to use science to help others, I will forever be grateful and proud to be part of the Ahituv Lab. Next, to Dr. Kevin Bender, my thesis chair and mentor. I am so thankful to have had the opportunity to learn the art and science of electrophysiology from you. I came to you with a background in behavior and you taught me the quantitative intricacies of squiggly lines all while singing Red Hot Chili Peppers and reminding me to breathe and savor the joys of science, I am proud to be a Bender Lab barnacle.

To Dr. Stephan Sanders, thank you for your guidance as a member of my thesis committee. Your work in ASD gene discovery was one of the reasons why I decided to pursue a PhD and I am still humbled that I was able to work and learn directly from you. To Dr. Georgia Panagiotakos, thank you for being my unbiased mentor and thesis

committee member. You provided me with immense comfort, strength and clarity, I am so thankful to have had the opportunity to work with you. To Dr. Navneet Matharu, I can't begin to thank you for not only teaching me the functional techniques essential to my research, but also for the nuances and skills of navigating graduate school and research. To Dr. Perry Spratt and Dr. Andrew Nelson, my teammates and partners in crime. There have been two times in my life when I've felt moved to tears by my excitement of science – the first when we rescued  $dV/dt$  in mice, and the next when we rescued in those stem cells. You were there in those life moments, and I am will forever cherish those experiences with you both. I am thankful to call you teammates through this marathon!

To the Ahituv Lab, specifically Ofer Yizhar-Barnea, Lana Harshman, Dianne Laboy Cintron, Xujia Zhou, Wei Gordon and Rachael Bradley. Thank you for supporting and helping me to grow as a research scientist, I can't imagine having more caring, smart, thoughtful and helpful lab mates. And thank you for always giving me the pink lab equipment first! To Arielle Shkedi, I am so thankful that we started this journey together from interviews and have come out with a lifelong friendship. To my PSPG classmates and colleagues you are all inspiring and I am so thankful for the opportunity to learn alongside of you all.

I would also like to thank Dr. Karen Parker at Stanford University, my first PI and the reason why I am a scientist. I would never have gotten this far without your direct mentorship and guidance. Thank you also to Dr. Antonio Hardan and Dr. Lawrence

Fung at the Autism and Developmental Disorder Research Program at the Stanford School of Medicine for encouraging and supporting me in pursuing a PhD.

Next, I'd like to thank my family. I am so blessed to have the love and support of my in-laws. Thank you to the Tamura's specifically Alva, Marcus, Russell, Lorae and Bob for accepting and enveloping me with love and support. I'd also like to thank my Aunt Janet, Uncle Bob and my cousins Morgan and Tess for being my home away from home and for filling me with warmth, comfort and delicious home cooked meals over the years. To my brothers Aaron and Nathan, you have both been my lifelong role models and heroes. You've taught me that following one's passion can move mountains and I am so proud to be your little sister. To Sandi and Hnin I'm so lucky to have the best sibling-in-laws and I am so thankful that you are a part of my life. To my nephews Porter and Pax, thank you for always helping me keep what's most important in perspective. Watching you two grow into your own beings is one of my life's greatest joys! To my parents Kimie and Kenneth Tanaka, thank you for everything you've done to help get me to this stage in my life. I move through this world because of the love and support you provided me, and I will never be able to express the extent of my gratitude.

Most importantly, to my husband Andrew, I couldn't have done this without you. Thank you for being so supportive and encouraging as I've navigated these last six years in graduate school. From odd work hours to taking care of Soma and Kuma to building me a new office for me to study in, to always making me laugh, you have been my rock and my everything. I love you so much and am so lucky to walk through this life with you!

## **Contributions**

Chapter 2: Perry Spratt, PhD and Andrew Nelson, PhD conducted the primary electrophysiological experiments. Henry Kyoung conducted the compartmental modeling and EEG work. Zizheng Li performed the intravenous tail vein injections.

“The important thing in following the path to Enlightenment is to avoid being caught and entangled in any extreme, that is, always to follow the Middle Way.”

- Lankavatara Sutra, The Teaching of Buddha



# Development of a CRISPR activation-based approach for the treatment of *SCN2A* haploinsufficiency in Autism Spectrum Disorder

Serena Tamura

## Abstract

Haploinsufficiency, having only one functional gene copy, is associated with 89 autism spectrum disorder (ASD) risk genes. Delivering functional gene copies via gene therapy could potentially restore transcriptional balance and rectify deficits in haploinsufficient diseases. Here, we tested whether *Cis*-Regulation therapy (CRT), a novel therapeutic approach that uses nuclease deficient gene-editing systems, such as a dead Cas9 (dCas9), fused to a transcriptional modulator/s to change the activity of a gene's regulatory elements for therapeutic benefit, could be a viable approach for treating ASD-associated haploinsufficiency regardless of gene size. Here, using *SCN2A* haploinsufficiency, a major ASD risk condition, we show that CRISPR activation (CRISPRa) of the existing functional copy is a viable therapeutic approach. First, we demonstrate the potential for a therapeutic to rescue electrophysiological deficits in mice by utilizing heterozygous *Scn2a* conditional knockin mice. Next, using an AAV-based CRISPRa approach, we rescue these electrophysiological deficits in *Scn2a* heterozygous mice and human *SCN2A* heterozygous excitatory neurons. Our results provide a novel therapeutic approach for numerous ASD-associated genes and suggest that rescuing *Scn2a* function, even in relatively mature developmental stages, could ameliorate neurodevelopmental phenotypes.

## Table of Contents

<b>Chapter 1: Introduction</b>	<b>1</b>
1.1 Introduction	2
<b>Chapter 2: CRISPR activation rescues electrophysiological abnormalities in SCN2A haploinsufficiency associated autism spectrum disorder</b>	<b>7</b>
2.1 Methods	8
2.2 Abstract	16
2.3 Results	18
2.4 Figures & Tables	26
<b>Chapter 3: Concluding Remarks</b>	<b>40</b>
3.1 Overview	41
3.2 Towards a Therapy and Future Directions	43
3.3 Conclusion	49
<b>References</b>	<b>50</b>

## List of Figures

Figure 1.1: <i>Cis</i> -regulation therapy using CRISPR activation schematic	28
Figure 2.1A: <i>Scn2a</i> <sup>+/<i>Kl</i></sup> inducible recovery mouse model genetic design	29
Figure 2.2: <i>Scn2a</i> <sup>+/<i>Kl</i></sup> cell specificity in excitatory pyramidal neurons	31
Figure 2.1B: AAV-Cre-mCherry injection schematic	29
Figure 2.1C: AAV-Cre-mCherry does not alter AP firing	29
Figure 2.1D: AAV-Cre-mCherry rescues peak dV/dt in <i>Cre</i> <sup>+</sup> neurons	29
Figure 2.1E: AAV-Cre-mCherry rescues backpropagating	29
Figure 2.1F: AAV-Cre-mCherry administration restores AMPA:NMDA	29
Figure 2.3A-B: <i>In vitro</i> sgRNA screening for mouse <i>SCN2A</i> CRISPRa	32
Figure 2.3C: <i>In vitro</i> off target analysis in Neuro-2A cells	32
Figure 2.4A: <i>Scn2a</i> -rAAV-CRISPRa local injection schematic	33
Figure 2.4B: Coronal section of locally injected <i>Scn2a</i> <sup>+/<i>-</i></sup> mice	33
Figure 2.4C: <i>In vivo</i> <i>Scn2a</i> mRNA fold change following local injection	33
Figure 2.4D: <i>Scn2a</i> -rAAV-CRISPRa has no effect on AP firing rates	33
Figure 2.4E: <i>Scn2a</i> -rAAV-CRISPRa rescues dV/dt in <i>Scn2a</i> <sup>+/<i>-</i></sup> mice	33
Figure 2.4F: <i>Scn2a</i> -rAAV-CRISPRa rescues AMPA:NMDA ratio	33
Figure 2.5A: <i>Scn2a</i> -rAAV-CRISPRa-PhP.eb systemic delivery schematic	35
Figure 2.5B: Sagittal section of intravenously treated <i>Scn2a</i> <sup>+/<i>-</i></sup> mice	35

<b>Figure 2.5C: Intravenous delivery of CRISPRa rescues dV/dt</b>	<b>35</b>
<b>Figure 2.5D: intravenous delivery of CRISPRa rescues AMPA:NMDA</b>	<b>35</b>
<b>Figure 2.5E: <i>In vivo</i> Scn2a mRNA fold change systemic injection</b>	<b>35</b>
<b>Figure 2.5F: Computational modeling of Scn2a mRNA expression</b>	<b>35</b>
<b>Figure 2.5G: Empirical measurements of peak dV/dt</b>	<b>35</b>
<b>Figure 2.5H: Baseline recordings of spike and wave discharge</b>	<b>35</b>
<b>Figure 2.5I: Low dose (20 mg/kg) of pentylentetrazole (PTZ)</b>	<b>35</b>
<b>Figure 2.5J: High dose (50 mg/kg) of pentylentetrazole (PTZ)</b>	<b>35</b>
<b>Figure 2.5K: High dose PTZ treatment survival curves</b>	<b>35</b>
<b>Figure 2.6A-B: <i>in vitro</i> sgRNA screening for human SCN2A</b>	<b>37</b>
<b>Figure 2.6C: hESC differentiated neuron strategy and schematic</b>	<b>37</b>
<b>Figure 2.6D: <i>in vitro</i> qPCR following differentiated neurons</b>	<b>37</b>
<b>Figure 2.7A: Schematic and differentiated neurons Immunofluorescence</b>	<b>38</b>
<b>Figure 2.7B-C: Action potential firing rates of differentiated neurons</b>	<b>38</b>
<b>Figure 2.7D-E: SCN2A-rAAV-CRISPRa shows partial dV/dt rescue</b>	<b>38</b>

## **List of Tables**

<b>Table 2.0: ASD risk gene cDNA length</b>	<b>26</b>
<b>Table 2.8: Primer and sgRNA sequences used in this dissertation</b>	<b>39</b>

## **Chapter 1: Introduction**

## 1.1: Introduction

Autism spectrum disorder (ASD) is a common neurodevelopmental disorder (NDD) and affects 1 in 54 school-aged children in the US (Maenner et al., 2020 & Elsabbagh et al., 2012). ASD is clinically diagnosed based on core deficits in social communication and restrictive or repetitive behaviors (Hyman et al., 2020). Previous efforts to elucidate the etiology of this disorder have been limited to a phenotype down study of complex behaviors associated with ASD. Recent advances in sequencing technologies and access to large ASD cohorts and simplex families (where only one individual in the family is affected with the disorder) have facilitated the identification of 102 high confidence ASD *de novo* risk genes. These genes are primarily involved in transcriptional regulation and neural communication during early brain development (Satterstrom et al., 2020). In addition, the majority of these risk genes (N=89) are thought to cause ASD due to haploinsufficiency (Satterstrom et al., 2020), having only one of two functional gene copies.

Amongst the aforementioned risk genes, *SCN2A* encoding the voltage-gated sodium channel alpha subunit 2 (Nav1.2) has the strongest association to ASD and contributes to over 10,000 cases in the US per year (0.3% of all ASD cases) (Sanders et al., 2015; Ben-Shalom et al., 2017). *SCN2A* loss of function (LoF) variants that result in haploinsufficiency cause one of the most common and significant genetically defined subsets of ASD and are comorbid with severe intellectual disability (ID) and poor developmental outcomes (Sanders et al., 2018; Ben-Shalom et al., 2017). There are 20

known *de novo* variants in the clinical population that cause haploinsufficiency. *De novo* gain of function mutations (GoF) in *SCN2A* are associated with two forms of epilepsy: benign infantile familial seizure (BIFS) and epileptic encephalopathy (EE) (Sanders et al., 2018).

*SCN2A* encodes the alpha subunit of the neuronal voltage-gated sodium channel  $Na_v1.2$ , which through numerous studies, primarily in mouse models, has been shown to perform different functions throughout development. Early in neuronal development, as axonal processes are elaborating and integrating into networks,  $Na_v1.2$  is the only sodium channel isoform expressed in the axon initial segment (AIS) of excitatory neurons and is essential for action potential (AP) firing (Boiko et al., 2003; Osorio et al., 2005; Gazina et al., 2015; Bender and Trussell, 2012). The AIS is an axonal sub compartment located proximal to the soma and is the site of dendritic signal accumulation and AP initiation. Following the first year of life in humans, which is equivalent to the first postnatal week in mice,  $Na_v1.2$  is replaced by  $Na_v1.6$  encoded by *SCN8A* in the distal AIS.  $Na_v1.6$  has a lower voltage threshold for activation (Kole et al., 2008; Kole and Stuart, 2012) and  $Na_v1.2$ , now restricted to the proximal AIS, takes on a new role as an AP signal booster rather than the sole initiator. At this stage in development, *Scn2a*<sup>+/-</sup> mice show peak action potential speed (dV/dt) deficits (reduced by 30%) compared to wild-type mice (Spratt et al., 2019).

Previous work by our group showed that  $Na_v1.2$  channels play an essential role beyond early development, after  $Na_v1.6$  takes over as AP signal initiator, by boosting signals



which assist in the maturation of glutamatergic neurons (Spratt et al., 2019). In adult wild-type mice,  $\text{Na}_v1.2$  channels in the proximal AIS backpropagates and boosts AP signals throughout the somatodendritic compartment of the glutamatergic neurons to promote activity-dependent synaptic maturation and refinement. Adult  $\text{Scn2a}^{+/-}$  mice also show impaired synaptic stability, as observed by lower AMPA:NMDA ratios in the synaptic spines of mature mice (Chater & Goda, 2014). Studies performed in  $\text{SCN2A}$  heterozygous excitatory neurons differentiated from human embryonic stem cells (hESC) have also demonstrated reduced spontaneous action potential spike rates in mutant heterozygous  $\text{SCN2A}^{+/-}$  excitatory neurons compared to wild-type differentiated excitatory neurons (Lu et al., 2019). In summary, mutations that cause  $\text{SCN2A}$  haploinsufficiency are thought to disrupt AP propagation early in life and impair dendritic excitability and synaptic function later in life.

For disorders caused by haploinsufficiency, including  $\text{SCN2A}$  haploinsufficiency, delivering additional gene copies via gene therapy represents a potential means of restoring gene expression levels and correcting ensuing deficits. For delivery, this technology usually relies on recombinant adeno-associated virus (rAAV) due to its limited pathogenicity and long-term transgene expression (Wang et al., 2019). However, the optimal packaging capacity of rAAV is 4.7 kb, limiting gene delivery to genes up to 3.5 kilobases (kb) in size, as additional sequences of ~ 1700 bp are also needed for transgene expression. Examination of cDNA length reveals that 40 of the 89 aforementioned haploinsufficient ASD genes, including  $\text{SCN2A}$ , exceed rAAV vector capacity (Table 2.0). To circumvent this problem, *Cis-Regulation* therapy (CRT) is a

novel therapeutic approach that modulates the activity of a gene's regulatory elements can be used to modify its expression for therapeutic benefit (Matharu & Ahituv, 2020). This strategy utilizes nuclease-deficient zinc fingers, TALEs or CRISPR to deliver transcriptional modulators to a gene's regulatory elements and modify its expression. These CRT modules fit within the rAAVs vector capacity, bypassing the cDNA packaging size limitations for standard gene therapy, thus offering an alternative therapeutic approach for gene dosage-associated conditions, such as haploinsufficiency. Previous work by our group utilized CRISPR activation (CRISPRa) CRT to rescue obesity in mice caused by haploinsufficiency of two different genes (Matharu et al., 2019).

Here, we tested whether CRT could be a viable therapeutic approach for ASD-associated haploinsufficiency using *SCN2A* as a model (**Fig. 1.1**). We first used a *Scn2a* heterozygous conditional knockin mouse to establish that activation of the wild-type *Scn2a* allele later in life could rescue electrophysiological deficits resulting from haploinsufficiency. We then optimized rAAV-based CRISPRa conditions to upregulate *Scn2a/SCN2A* both in mice and humans by targeting its promoter. Injection of mouse rAAV-CRISPRa into the medial prefrontal cortex (mPFC) of *Scn2a<sup>+/-</sup>* mice upregulated the expression of the existing functional copy of *Scn2a*. CRISPRa-treated *Scn2a<sup>+/-</sup>* mice showed a functional rescue in peak action potential firing speed and AMPA:NMDA ratios, showcasing a restoration in activity-dependent synaptic maturation. To further link these findings to a viable therapeutic, excitatory neuron differentiated from hESCs were treated with human rAAV-CRISPRa. Treated human-derived *SCN2A<sup>+/-</sup>* excitatory

neurons showed improved firing rates and action potential peak speed compared to untreated neurons. This work provides a potential therapeutic approach for multiple haploinsufficiency-associated ASD genes and suggests that rescue later in life could ameliorate electrophysiological phenotypes associated with NDDs.

**Chapter 2:**  
**CRISPR activation rescues electrophysiological abnormalities in *SCN2A***  
**haploinsufficiency associated autism spectrum disorder**

## 2.1: Methods

### CRISPRa *in vitro* optimization

Ten sgRNAs targeting the mouse *Scn2a* or human *SCN2A* promoters were designed using the Broad Institute's GPP sgRNA Design Tool (Genetic Perturbation Platform, Broad Institute). These guides were then individually cloned into pAAV-U6-sasgRNA-CMV-mCherry-WPREpA at the *Bst*XI and *Xho*I restriction enzyme sites using the In-Fusion HD cloning kit (Clontech). To generate AAV vectors pcDNA-dCas9-VP64 (Addgene # 47107), and U6-sgRNA-CMV-mCherry-WPREpA were cloned replacing the Ef1a-FAS-hChr2(H134R)-mCherry-WPRE-pA with U6-sgRNA-CMV-mCherry-WPREpA into the backbone of pAAV-Ef1a-FAS-hChr2(H134R)- mCherry-WPRE-pA (Addgene #37090). Mouse sgRNAs were tested in the neuroblastoma cell line Neuro-2A (ATCC CCL-131) and human sgRNAs in the neuroblastoma cell line SH-SY5Y (ATCC CRL-2266 ). Cell lines were maintained following ATCC guidelines. Cells were transiently co-transfected with individual sgRNA cloned into pAAV-U6-sasgRNA- CMV-mCherry-WPREpA along with pCMV-sadCas9-VP64 for 48 hours using Opti-MEM Reduced Serum Medium (Thermo Fisher 31985088) and X-tremeGENE HP (Sigma-Aldrich). RNA was isolated using the RNEASY MINI Kit (Qiagen 74104) following the manufacturer's protocol. cDNA was synthesized using SuperScript III First-Strand Synthesis System (Invitrogen 18080051) and qPCR was conducted using SsoFast EvaGreen Supermix (Bio-Rad) and was analyzed using the  $\Delta\Delta$ CT methods comparing a no sgRNA transfection normalized to Actb as a housekeeping gene. AAVs were produced at the Stanford Gene Vector and Viral Core.

### ***In vivo* AAV administration**

For local AAV administration, C57/BL6 mice aged P30-P40 were anesthetized using isoflurane inhalation anesthesia at 0.5-2.0% and mounted onto a stereotaxic apparatus or frame (Kopf 1900). 500 nL of AAV was injected into the mPFC at stereotaxic coordinates from bregma [mm]: anterior-posterior [AP], +1.7, mediolateral [ML] -0.35; dorsoventral [DV]: -2.6 at a viral infusion rate of 0.1  $\mu\text{L min}^{-1}$ . For systemic AAV administration, mice aged P30-P40 were kept on a 37C heating pad and harnessed using a brass mouse restrainer (SAI Infusion Tech). Lateral tail vein injections were carried out with AAV ( $1 \times 10^{11}$  vg/mouse) suspended in 200  $\mu\text{L}$  saline using a 30G needle. Following injection, mice were used for subsequent experiments four weeks post injection.

### **Mouse Husbandry and Genotyping**

*Scn2a*<sup>+/-</sup> mice were provided by Drs. E. Glasscock and M. Montal (Mishra et al., 2017; Planells-Cases et al., 2000). All mice and associated experimental procedures were performed in accordance with UCSF IACUC guidelines. Genotyping was performed on DNA extracted from tail clips using the KAPA Mouse Genotyping Kit (Roche #07961766001). See (Table 2.8) for primer sequences.

### **Tissue dissection**

Four weeks post-injection mouse brain were carefully extracted and 250  $\mu\text{m}$  thick coronal slices containing the mPFC were dissected in artificial cerebrospinal solution containing (in mM): 87 NaCl, 25 NaHCO<sub>3</sub>, 25 glucose, 75 sucrose, 2.5 KCl, 1.25

NaH<sub>2</sub>PO<sub>4</sub>, 0.5 CaCl<sub>2</sub> and 7 MgCl<sub>2</sub>; bubbled with 5%CO<sub>2</sub>/95%O<sub>2</sub>; 4C. Fluorescence mCherry expression in the mPFC of the injected hemisphere was validated using a fluorescent stereomicroscope (NIKON SMZ1500). For mRNA expression analyses, both the injected (mCherry positive) and uninjected hemisphere (mCherry negative) were dissected using a sterile miltex disposable punch biopsy (Medline MIL3332P25) and flash frozen in RLT lysis buffer (Qiagen). RNA was extracted using the RNEasy Micro Kit following the manufacturer's protocol (Qiagen). cDNA and downstream qPCR was conducted using SuperScript III (Invitrogen) and SsoFast EvaGreen Supermix (Bio-Rad). qPCR results comparing the injected and uninjected hemispheres were conducted using the  $\Delta\Delta$ CT methods and normalized to Actb as a housekeeping gene.

#### **human embryonic stem cell (hESC) differentiation and maturation protocol**

Wildtype and *SCN2A*<sup>+/-</sup> HUES66 (NIH Registration #0057) hESC cell lines were obtained from the Harvard Stem Cell Institute and plated on Matrigel (Corning) coated standard tissue culture plates and maintained in mTESR (STEMcell technologies). The STEMdiff SMADi Embryoid Body Neural Induction protocol (STEMcell Tech) was used according to manufacturer instructions to generate neural progenitor cells (NPCs) following a similar strategy in (Ruden et al., 2021). NPCs were further differentiated into neuronal forebrain precursors using the STEMdiff ForeBrain Neuron Differentiation protocol (Document #10000005464, Stemcell Technologies, Vancouver, CanadaSTEMcell Tech), and neuronal precursors underwent maturation into forebrain neurons using the STEMdiff Forebrain Maturation Kit with BrainPhys (STEMCell Tech).

Neuronal differentiation and maturation was conducted on Poly-L-Ornithine (PLO)-Laminin coated German coverslips (Neuvitro GG-25-1.5-Laminin) for 65 days.

### **Immunofluorescence**

Differentiated neurons were fixed at DIV 65 in 4% PFA and 4% sucrose and blocked with 10% Normal Goat Serum in PBST. Cells were incubated with primary antibodies directed against MAP2 (Invitrogen, PA1-10005, 1:5000), GFAP (Abcam, ab7260, 1:1000) and Ankyrin-G (Neuromab, 75-146, 1:1000) overnight at 4 degrees. Cells were then incubated with the secondary antibodies Goat anti-Chicken IgY (H+L) Cross-Adsorbed Secondary Antibody, Alexa Fluor Plus 647 (Invitrogen A32933) at 1:500 and Goat anti-Mouse IgG (H+L) Highly CrossAdsorbed Secondary Antibody, Alexa Fluor 488 (Thermo Fisher A-11029) at 1:500. Immunostained cells were then mounted on coverslips with ProLong™ Diamond Antifade Mountant with DAPI (Thermo Fisher P36962). Images were captured with a 40x 1.4NA objective using an Olympus Fluoview FV3000 confocal microscope.

### ***Ex Vivo* Electrophysiology and 2-photon imaging**

All *ex vivo* electrophysiology and 2-photon imaging was acquired and performed using the same methods as previously described (Spratt et al., 2019). Mice were anesthetized using isoflurane and 250 µm coronal slices were prepared. Cutting solution contained (in mM): 87 NaCl, 25 NaHCO<sub>3</sub>, 25 glucose, 75 sucrose, 2.5 KCl, 1.25 NaH<sub>2</sub>PO<sub>4</sub>, 0.5 CaCl<sub>2</sub> and 7 MgCl<sub>2</sub>; bubbled with 5%CO<sub>2</sub>/95%O<sub>2</sub>; 4°C. Following cutting, slices were either incubated in the same solution or in the recording solution for 30 min at 33°C,



then at room temperature until recording. Recording solution contained (in mM): 125 NaCl, 2.5 KCl, 2 CaCl<sub>2</sub>, 1 MgCl<sub>2</sub>, 25 NaHCO<sub>3</sub>, 1.25 NaH<sub>2</sub>PO<sub>4</sub>, 25 glucose; bubbled with 5%CO<sub>2</sub>/95%O<sub>2</sub>; 32–34°C, ~310 mOsm. Neurons were visualized with differential interference contrast (DIC) optics for conventional visually guided whole-cell recording, or with 2-photon-guided imaging of reporter-driven mCherry fluorescence overlaid on an image of the slice (scanning DIC). For current-clamp recordings and voltage-clamp recordings of K<sup>+</sup> currents, patch electrodes (Schott 8250 glass, 3–4 MΩ tip resistance) were filled with a solution containing (in mM): 113 K-Gluconate, 9 HEPES, 4.5 MgCl<sub>2</sub>, 0.1 EGTA, 14 Tris2-phosphocreatine, 4 Na<sub>2</sub>-ATP, 0.3 tris-GTP; ~290 mOsm, pH: 7.2–7.25. For Ca<sup>2+</sup> imaging, EGTA was replaced with 250 μM Fluo-5F and 20 μM Alexa 594. For voltage-clamp recordings of persistent Na<sup>+</sup> currents and synaptic activity, internal solution contained (in mM): 110 CsMeSO<sub>3</sub>, 40 HEPES, 1 KCl, 4 NaCl, 4 Mg-ATP, 10 Na-phosphocreatine, 0.4 Na<sub>2</sub>-GTP, 0.1 EGTA; ~290 mOsm, pH: 7.22. All data were corrected for measured junction potentials of 12 and 11 mV in K- and Cs-based internals, respectively.

Electrophysiological data were acquired using Multiclamp 700A or 700B amplifiers (Molecular Devices) via custom routines in IgorPro (Wavemetrics). For measurements of action potential waveform, data were acquired at 50 kHz and filtered at 20 kHz. For all other measurements, data were acquired at 10–20 kHz and filtered at 3–10 kHz. For current-clamp recordings, pipette capacitance was compensated by 50% of the fast capacitance measured under gigaohm seal conditions in voltage-clamp prior to establishing a whole-cell configuration, and the bridge was balanced. For voltage-clamp

recordings, pipette capacitance was compensated completely, and series resistance was compensated 50%. Series resistance was  $<15 \text{ M}\Omega$  in all recordings. Experiments were omitted if input resistance changed by  $> \pm 15\%$ . Two-photon laser scanning microscopy (2PLSM) was performed as previously described (Bender and Turssell, 2009). A 2-photon source (Coherent Ultra II) was tuned to 810 nm for morphology and calcium imaging. Epi- and transfluorescence signals were captured either through a 40 $\times$ , 0.8 NA objective for calcium imaging or a 60 $\times$ , 1.0 NA objective for spine morphology imaging, paired with a 1.4 NA oil immersion condenser (Olympus). Fluorescence was split into red and green channels using dichroic mirrors and band-pass filters (575 DCXR, ET525/70m-2p, ET620/60m-2p, Chroma). Green fluorescence (Fluo-5F) was captured with 10770–40 photomultiplier tubes selected for high quantum efficiency and low dark counts (PMTs, Hamamatsu). Red fluorescence (Alexa 594) was captured with R9110 PMTs. Data were collected in linescan mode (2–2.4 ms/line, including mirror flyback). For calcium imaging, data were presented as averages of 10–20 events per site, and expressed as  $\Delta(G/R)/(G/R)_{\text{max}} \times 100$ , where  $(G/R)_{\text{max}}$  was the maximal fluorescence in saturating  $\text{Ca}^{2+}$  (2 mM) (Yasuda et al., 2004). Backpropagation experiments were performed in 25  $\mu\text{M}$  picrotoxin, 10  $\mu\text{M}$  NBQX and 10  $\mu\text{M}$  R-CPP.

### **EEG Implant Surgeries**

Mice were anesthetized with isoflurane and placed on a stereotaxic apparatus. Screws with wire leads were implanted in 2-3 turns into five burr holes at (stereotaxic coordinates relative to bregma [mm]) PFC: 1.7 anterior-posterior (AP), -0.3 mediolateral (ML); S1: -

1.8 AP, 2.5 ML; reference and ground: -5 AP, 0.9 ML (Pinnacle Technology). A head mount was then attached to the wire leads and secured in adhesive dental cement. Mice were given at least one week for post-surgery recovery prior to EEG recordings.

### **EEG Recordings**

EEG recordings were performed using the Sirenia Acquisition Software (Pinnacle Technology) at 2 kHz sampling frequency with simultaneous video capture. Pentylentetrazol (PTZ) administration of low (20 mg/kg) and high (50 mg/kg) doses were performed in two separate sessions at least two weeks apart to minimize the kindling effect. PTZ solutions were prepared fresh at the start of every recording day. For each session, baseline activity was recorded for 30 minutes after which the mice were injected with PTZ via intraperitoneal injection and continued recording for 40 minutes. Recordings were performed between 10 AM and 6 PM to control for the circadian light-dark cycle.

### **EEG Analysis**

All analyses were performed offline using custom software written in Python. Preprocessing was first performed on baseline and low dose PTZ recordings including a bandpass filter between 1-100 Hz before downsampling to 200 Hz. Spectral power was computed using the continuous wavelet transform (CWT) with a complex Morlet wavelet. The recording was segmented into 125 ms windows and classified as part of a spike-wave discharge (SWD) based on the amplitude of spikes and the spectral power. The band power of interest was calculated as the 3-7 Hz band subtracted by the 0-1 Hz band to eliminate non-SWD frequencies. Spikes in the EEG signal were detected based on an

amplitude threshold set at 3 times the root mean square of baseline, and the power threshold was set at 3 times the band power in the first minute of baseline. SWDs were considered events with durations lasting at least 1 sec and verified by manual inspection.

Seizure scoring for high dose PTZ recordings were measured from simultaneous video and EEG monitoring. Behavioral classification of increasing seizure severity was based on the Racine scale and a previous report of PTZ-induced seizures (Van Erum et al., 2019 & Miyamoto et al., 2019). Latency to seizure activity was considered the time from PTZ administration to the first occurrence of the seizure. Behavioral arrest was defined as a sudden immobilization accompanied by spike-wave discharges. A myoclonic jerk was defined as a neck or body twitch accompanied by a single sharp spike in the EEG signal. A clonic seizure was defined as clonic convulsions while retaining righting reflex with high amplitude spiking in the EEG signal. A tonic-clonic seizure was defined as clonic convulsions leading to wild jumping also with high amplitude spiking in the EEG signal. The animal was considered dead when the tonic-clonic seizure led to tonic extension of hind limbs followed by loss of body tone and close to flat EEG signal.

### **Computational Compartmental Modeling**

A pyramidal cell compartmental model was implemented in the NEURON environment (v7.7) based on the Blue Brain Project thick-tufted layer 5b pyramidal cell (TTPC1) model used in our previous study (Markram et al., 2015; Spratt et al., 2021; Ben-Shalom et al., 2017). The TTPC1 model was adjusted to include an AIS, and the original Na channels in the TTPC1 model were replaced with  $Na_v1.2$  and  $Na_v1.6$  channels in compartments with densities as described previously (Ben-Shalom et al., 2017).

## 2.2: Abstract

Eighty-seven percent of high-confidence ASD risk genes are thought to cause ASD due to haploinsufficiency, with *SCN2A* haploinsufficiency being one of the most significant genetically defined subsets of ASD (Ben-Shalom et al., 2017). Here, we show how CRT using CRISPR activation could be used to rescue the electrophysiological deficits associated with *SCN2A* haploinsufficiency. Using a genetically engineered conditional knockin mouse line, we first demonstrate the feasibility of *Cre*-induced transgenic rescue of *Scn2a* haploinsufficiency in adolescent mice.

A major goal of CRT is to achieve physiologically normal levels of the modulated gene that are therapeutically beneficial. Obtaining levels that are too high could also have deleterious phenotypic effects and levels that are too low may not have therapeutic benefit. For *SCN2A*, this is of particular importance, as GoF mutations are known to cause hyperexcitability and manifest in two forms of epilepsy: benign infantile familial seizure (BIFS) and epileptic encephalopathy (EE) (Sanders et al., 2018). Here, we intentionally used VP64 as the transcriptional activator in part due to its small size allowing it to fit within an rAAV vector, but also to achieve physiologically relevant mRNA expression (Chavez et al., 2016).

Upregulation of *Scn2a* in adult *Scn2a*<sup>+/-</sup> mice by direct stereotaxic injection into the mPFC or intravenous tail vein delivery of *Scn2a*-rAAV-CRISPRa restored action potential firing speed. *Scn2a*-rAAV-CRISPRa also improved quantitative markers of

synaptic maturation in *Scn2a*<sup>+/-</sup> mice, as measured by AMPA:NMDA ratio. rAAV-CRISPRa transduction of excitatory neurons derived from hESC heterozygous for *SCN2A* rescued the reduction in spike firing rate resulting from *SCN2A* haploinsufficiency and improved the action potential firing speed compared to untreated wild-type neurons. This data suggest that CRT is a viable approach for treating *SCN2A* haploinsufficiency.

## 2.3: Results

### Restoration of two functional *Scn2a* copies in adolescent mice rescues electrophysiological deficits

To test the feasibility of CRISPRa to rescue deficits associated with haploinsufficiency, we first developed a knockin mouse line that can assess the efficacy of *Scn2a* allele restoration from haploinsufficient conditions (termed *Scn2a<sup>+KI</sup>*). In this mouse, exons 3-5 of the *Scn2a* gene are flipped and flanked by LoxP sites, with eGFP in frame to visualize cells that express *Scn2a* (**Fig. 2.1A**). In the neocortex, *Scn2a* is primarily expressed in excitatory neurons. Constitutive heterozygous LoF mutations in *Scn2a* reduces the speed of the rising phase of the action potential (AP), impairs AP-evoked dendritic calcium electrogenesis, and affects excitatory synapse function, resulting in an excess of silent synapses more commonly observed in less mature neurons (Spratt et al., 2019). Converting a heterozygous *Scn2a<sup>+KI</sup>* mouse into a wild-type mouse with a *Cre* injection would determine whether rescuing haploinsufficiency of *Scn2a* is a feasible approach to restoring the associated electrophysiological deficits in adolescent mice. Confocal imaging of neocortical pyramidal neurons in *Scn2a<sup>+KI</sup>* animals revealed that the GFP+ neurons were indeed only expressed in excitatory pyramidal cells and were distinct from parvalbumin-positive (PV+) GABAergic interneurons. This suggests cell-specificity of allele restoration in rescuing *Scn2a* haploinsufficiency in excitatory GFP+ neurons (**Fig. 2.2**).

To test for the feasibility of a phenotypic rescue in adolescence, we injected rAAV-EF1 $\alpha$ -Cre-mCherry into the medial prefrontal cortex (mPFC) of these *Scn2a<sup>+KI</sup>* mice at

postnatal day (P) 30-40 (**Fig. 2.1B**). Four weeks post injection, mCherry+ and GFP- neurons were targeted for whole-cell recordings in acute slices. We then looked at two measures of intrinsic excitability, AP firing rate and peak dV/dt, which is a measure of AP velocity at the soma. We found no significant difference in AP firing rates between *Cre*+ and *Cre*- neurons (via mCherry fluorescence), which is consistent with the firing rates of constitutive wild-type and *Scn2a*<sup>+/-</sup> mice (**Fig. 2.1C**). Next, we measured peak dV/dt, which is known to be reduced in constitutive *Scn2a*<sup>+/-</sup> and was also found to be reduced in *Scn2a*<sup>+/*Kl*</sup> mice compared to wild-type mice (Spratt et al., 2019). *Cre*+ neurons in *Scn2a*<sup>+/*Kl*</sup> mice fired peak dV/dt in *Cre*+ neurons at rates comparable to that of constitutive wild-type cells. In contrast, *Cre* negative neurons continued to fire at a dV/dt deficit consistent with constitutive *Scn2a*<sup>+/-</sup> neurons (**Fig. 2.1D**). No changes in AP threshold were observed between these groups (**Fig. 2.1D**). In addition to rescuing dV/dt, AP backpropagation (bAP) was also rescued in *Cre*+ neurons when administered to *Scn2a*<sup>+/*Kl*</sup> mice (**Fig. 2.1E**). Na<sub>v</sub>1.2 plays an essential role in promoting the bAP of action potentials within neocortical pyramidal cell dendrites (Spratt et al., 2019). bAP provides input signals that regulate excitatory synaptic function and dendritic excitability, which can be measured by the AMPA:NMDA ratio. *Cre*+ neurons showed a rescue of the AMPA:NMDA ratio suggesting the restoration of synaptic strength and maturation (**Fig. 2.1F**). Together, this data show that all features of intrinsic and synaptic function were restored to wild-type levels upon reactivation of the second allele in adolescent stages and that *Scn2a* has a life-long role in maintaining pyramidal cell dendritic excitability, and that *Scn2a* has a life-long role in maintaining pyramidal cell dendritic excitability. These results suggest that upregulation of *Scn2a* during adolescence could



be a viable therapeutic approach to restoring excitability and ameliorating synaptic deficits in *Scn2a* haploinsufficient mice.

### ***Scn2a*-CRISPRa optimization *in vitro***

To optimize mouse *Scn2a* CRISPRa constructs, we tested the ability of nine different sgRNAs targeting the *Scn2a* promoter along with a *Staphylococcus aureus* (sa) dCas9 fused to the transcriptional activator VP64 to upregulate *Scn2a* in mouse neuroblastoma cells (Neuro-2a) (**Fig 2.3A**). The VP64 transcriptional activator was selected due to its small size, allowing it to fit into an rAAV vector, and due to its modest upregulation potential, which has been shown to provide close to physiological wild-type levels in mice heterozygous for other forms of haploinsufficiency (Matharu et al., 2019). Forty-eight hours post transfection, *Scn2a* mRNA expression was measured by quantitative polymerase chain reaction (qPCR), finding three sgRNAs that significantly increase *Scn2a* mRNA expression compared to a no sgRNA transfection condition (**Fig. 2.3A**). We packaged these three sgRNAs and the transcriptional activator plasmid into the rAAV-DJ serotype, as it provides strong neuronal expression (Haery et al., 2019). rAAV-sgRNA viruses were then co-transduced with the rAAV-sadCas9-VP64 activator into Neuro-2a cells for five days. One of the three rAAV-sgRNA was found to significantly increase *Scn2a* mRNA expression by two-fold and was selected for subsequent mouse studies (**Fig. 2.3B**). To test for off-target effects, we measured mRNA expression changes following plasmid CRISPRa transfection in Neuro-2a cells via qPCR on sodium channels within the same topologically associated domain (TAD). We excluded *Scn7a* in this analysis due to its low endogenous expression levels in this cell type. We

observed that *Scn2a* was the only significantly upregulated central nervous system (CNS) related sodium channel compared to cells transfected with a no sgRNA negative control (**Fig. 2.3C**).

### **Administration of CRISPRa restores cell-autonomous excitability in *Scn2a*<sup>+/-</sup> mice**

To test whether *Scn2a*-rAAV-CRISPRa (rAAV-sadCas9-VP64 + rAAV-*Scn2a*-sgRNA) could be used as a therapeutic intervention for *Scn2a* haploinsufficiency in adolescent mice, we stereotactically injected these constructs into the medial prefrontal cortex (mPFC) of constitutive *Scn2a*<sup>+/-</sup> mice at postnatal day (P) 30-40 (**Fig. 2.4A**). Wild-type and *Scn2a*<sup>+/-</sup> mice were injected unilaterally in one hemisphere and the opposite hemisphere was used as a biologically matched uninjected control (**Fig. 2.4B**). As a negative (no sgRNA) control, wild-type and *Scn2a*<sup>+/-</sup> mice were co-injected with rAAV-sadCas9-VP64 along with an rAAV-mCherry (termed rAAV-empty-mCherry or empty). Four weeks following injection, the mPFC of the injected and uninjected hemispheres were dissected and extracted for qPCR analysis and electrophysiological recordings. *Scn2a*<sup>+/-</sup> mice and wild-type mice injected with *Scn2a*-rAAV-CRISPRa showed an upregulation of *Scn2a* mRNA of around 1.5 fold and 1.7 fold, respectively, compared to the uninjected hemisphere (**Fig. 2.4C**). rAAV-empty-mCherry injected mice showed no upregulation of *Scn2a* mRNA expression in either *Scn2a*<sup>+/-</sup> or wild-type mice compared to its respective uninjected hemispheres (**Fig. 2.4C**).

Cells treated with *Scn2a*-rAAV-CRISPRa had no effect on AP firing rates between WT and *Scn2a*<sup>+/-</sup> mice, which was also consistent with firing rates between WT and

constitutive *Scn2a*<sup>+/-</sup> mice treated with rAAV-empty-mCherry (**Fig. 2.4D**). Neurons from constitutive *Scn2a*<sup>+/-</sup> mice fire action potentials that are 30% slower than neurons from wild-type mice. *Scn2a*-rAAV-CRISPRa was able to rescue this 30% deficit in somatic *Scn2a* function in treated *Scn2a*<sup>+/-</sup> mice by restoring peak dV/dt (**Fig. 2.4E**). Moreover, examination of excitatory synaptic function in *Scn2a*-rAAV-CRISPRa treated *Scn2a*<sup>+/-</sup> mice, showed a rescue of the AMPA:NMDA ratio comparable to levels seen in mature wild-type neurons (**Fig. 2.4F**). These results suggest that upregulation of the existing single copy of *Scn2a* via CRISPRa can rescue synaptic deficits in adolescent mice.

### **Systemic rAAV-CRISPRa administration restores electrophysiological deficits in *Scn2a*<sup>+/-</sup> mice**

We next explored the feasibility of a more clinically translatable delivery approach through intravenous systemic delivery of *Scn2a*-rAAV-CRISPRa in mice. *Scn2a*<sup>+/-</sup> mice were tail vein injected with *Scn2a*-rAAV-CRISPRa constructs packaged using the PhP.eb rAAV serotype, which can readily pass through the blood brain barrier in C57BL/6 mice and provide robust brain transgene expression (Deverman et al., 2016). Mice were injected via lateral tail vein at P30-40 and after four weeks showed widespread infectivity in the brain (**Fig. 2.5A and 2.5B**). qPCR showed a 2.1-fold upregulation of *Scn2a* mRNA expression in treated *Scn2a*<sup>+/-</sup> compared to age-matched untreated heterozygous and wild-type mice respectively (**Fig. 2.5E**).

Electrophysiological analysis of *Scn2a*-rAAV-CRISPRa-Php.eb tail vein injected *Scn2a*<sup>+/-</sup> mice show a rescue in waveform, dV/dt and AMPA:NMDA comparable to that of local stereotactic *Scn2a*-rAAV-CRISPRa treatment directly into the mPFC (**Fig. 2.5C and 2.5D**) Together, this data suggests the feasibility of systemic administration of

rAAV-CRISPRa to rescue *Scn2a* haploinsufficiency associated electrophysiological defects.

### **Upregulation of *Scn2a* in wild-type mice does not induce cellular or behavioral hyperexcitability**

Increased channel function, due to gain of function mutations in *SCN2A*, are associated with epileptic encephalopathy (Reynolds et al., 2019). Thus, a major therapeutic concern of using CRISPRa to rescue *SCN2A* haploinsufficiency is overexpression beyond normal physiologically levels, which could lead to hyperexcitability and seizures. To test this, we upregulated *Scn2a* in wild-type mice and analyzed them for any electrophysiological abnormalities. Similar to the aforementioned heterozygous mice, we unilaterally injected *Scn2a*-rAAV-CRISPRa into the medial prefrontal cortex (mPFC) at P30-40 and analyzed them four weeks post injection. We observed an average of 1.7 fold upregulation of *Scn2a* mRNA compared to the uninjected hemisphere (**Fig. 2.4C**). Measurements of AP peak  $dV/dt$  in wild-type neurons treated with *Scn2a*-rAAV-CRISPRa showed identical values of AP velocity as untreated wild-type cells despite having higher gene expression levels (**Fig. 2.5G**). These data suggest that *Scn2a*-rAAV-CRISPRa does not induce neuronal hyperexcitability, contradictory to a computational compartmental model (**Fig 2.5F**).

As seizures are a key feature of *SCN2A* channel excitability, we next tested whether *Scn2a* overexpression via CRISPRa in both wild-type and heterozygous mice results in seizures. We examined absence-like seizure phenotypes by measuring spike and wave

discharges (SWD), which are common and documented to occur at a low frequency in C57BL/6 mice (Fig. 2.5H). We observed no difference in SWD frequency in wild-type, *Scn2a*<sup>+/-</sup> or wild-type and *Scn2a*<sup>+/-</sup> mice treated with *Scn2a*-rAAV-CRISPRa at baseline and when challenged with a low dose (20 mg/kg) of pentylenetetrazole (PTZ), a known seizure inducing pharmacological drug (Fig. 2.5H-I). We next assessed whether a more clinically relevant seizure form, similar to what is documented in the SCN2A GoF epileptic encephalopathy population, is observed in these mice. We challenged them with a high dose of PTZ (50 mg/kg) to induce myoclonic jerks and tonic clonic seizures (Fig. 2.5J). Similar to the low dose treatment, we saw no difference in survival amongst constitutive or CRISPRa treated wild-type and *Scn2a*<sup>+/-</sup> mice following a high dose of PTZ that invokes tonic clonic seizures (Fig. 2.5K).

### **CRISPRa rescues firing patterns in excitatory neurons derived from SCN2A<sup>+/-</sup> hESC**

To further investigate the translational potential of this approach, we tested the ability of SCN2A-rAAV-CRISPRa to rescue electrophysiological phenotypes of SCN2A<sup>+/-</sup> neurons differentiated from human embryonic stem cells (hESCs). sgRNA constructs that target the human SCN2A promoter were designed in a similar strategy to that of the mouse and screened for upregulation of SCN2A in a human neuroblastoma cell line (SH-SY5Y). One sgRNA out of ten was found to increase SCN2A mRNA by 1.5-fold after a transient co-transfection and 1.3-fold following rAAV-DJ serotype infection (Fig. 2.6A-B). We procured previously characterized SCN2A<sup>+/-</sup> hESC lines; previous studies demonstrated a reduction in spontaneous spike rate in excitatory neurons derived from

these hESC lines compared to wild-type hESC derived excitatory neurons (Lu et al., 2019). hESCs were differentiated into excitatory neurons using the SMADi STEMDiff forebrain differentiation and maturation protocol (**Fig. 2.6C**) following a similar protocol outlined in (Ruden et al., 2021). Differentiated neurons were grown on coverslips and treated with *SCN2A*-rAAV-human-CRISPRa at maturation day *in vitro* (DIV) 30 and phenotyped at maturation DIV 65 (**Fig. 2.7A**). Immunostaining of cells at DIV 65 with MAP2 and GFAP showed efficient differentiation into excitatory neurons and supporting glial cells respectively (**Fig. 2.7A**). DIV 65 matched *SCN2A*<sup>+/-</sup> neurons treated with *SCN2A*-rAAV-CRISPRa showed an upregulation of *SCN2A* mRNA by 0.98 fold compared to untreated wild-type *SCN2A* neurons (**Fig. 2.6D**). Examination of AP firing rates showed that *SCN2A*<sup>+/-</sup> differentiated neurons had a significant reduction in firing rates compared to wild-type differentiated neurons (**Fig. 2.7B-C**). In contrast, *SCN2A*-rAAV-CRISPRa treated neurons showed a significant rescue of AP firing rates (). In addition, while *SCN2A*<sup>+/-</sup> neurons fired peak dV/dt at 24 V/sec, *SCN2A*<sup>+/-</sup> neurons treated with *SCN2A*-rAAV-CRISPRa fired peak dV/dt at around 70 V/sec (**Fig. 4D**), which was more comparable to wild-type cells (125 V/sec) (**Fig. 2.7D-E**). Together, these data suggest that CRISPRa can provide a potential therapeutic intervention for *SCN2A* haploinsufficiency in human neuronal cell types.

## 2.4: Figures & Tables

**Table 2.0:** Coding Sequence (CDS) length of 89 high confidence risk genes associated with ASD due to haploinsufficiency. Highlighted are those genes that exceed rAAV base pair capacity (>/ 3500 base pairs).

hugoGene	Gene ID	Transcript ID	CDS Length (bp)
CHD8	ENSG00000100888	ENST00000430710	7746
SCN2A	ENSG00000136531	ENST00000631182	6018
SYNGAP1	ENSG00000227460	ENST00000629380	4032
ADNP	ENSG00000101126	ENST00000621696.5	3309
FOXP1	ENSG00000114861	ENST00000318789	2082
POGZ	ENSG00000143442	ENST00000271715.7	4233
ARID1B	ENSG00000049618	ENST00000647938.1	6750
KMT5B	ENSG00000110066	ENST00000304363.9	2658
DYRK1A	ENSG00000157540	ENST00000398960	2292
SLC6A1	ENSG00000157103	ENST00000287766.10	1800
GRIN2B	ENSG00000273079	ENST00000609686	4455
PTEN	ENSG00000171862	ENST00000371953	1212
SHANK3	ENSG00000251322	ENST00000262795	5193
MED13L	ENSG00000123066	ENST00000281928	6633
GIGYF1	ENSG00000146830	ENST00000678049.1	3108
CHD2	ENSG00000173575	ENST00000577670	5487
ANKRD11	ENSG00000167522	ENST00000301030	7992
ANK2	ENSG00000145362	ENST00000503423	11874
ASH1L	ENSG00000116539	ENST00000392403.8	8895
TLK2	ENSG00000146872	ENST00000346027	2319
CTNNB1	ENSG00000168036	ENST00000349496.11	2346
KDM6B	ENSG00000132510	ENST00000254846.9	5049
DSCAM	ENSG00000171587	ENST00000400454.5	6039
SETD5	ENSG00000168137	ENST00000402198	4386
KCNQ3	ENSG00000184156	ENST00000388996.10	2619
SRPRA	ENSG00000182934	ENST00000332118.11	1917
WAC	ENSG00000095787	ENST00000354911.9	1944
SHANK2	ENSG00000162105	ENST00000338508.8	3786
NRXN1	ENSG00000179915	ENST00000401669	4644
TBL1XR1	ENSG00000177565	ENST00000457928.7	1545
MYT1L	ENSG00000186487	ENST00000428368	3624
RORB	ENSG00000198963	ENST00000376896.8	1380
RAI1	ENSG00000108557	ENST00000353383	5721
DYNC1H1	ENSG00000197102	ENST00000360184.10	13941
DPYSL2	ENSG00000092964	ENST00000521913.7	2034
AP2S1	ENSG00000042753	ENST00000263270.11	429
KMT2C	ENSG00000055609	ENST00000262189.11	14736
PAX5	ENSG00000196092	ENST00000358127	1176
GABRB3	ENSG00000166206	ENST00000311550.10	1422
SIN3A	ENSG00000169375	ENST00000360439	3822
MBD5	ENSG00000204406	ENST00000407073	5184
MAP1A	ENSG00000166963	ENST00000300231.6	8412
STXBP1	ENSG00000136854	ENST00000373299	1812
CELF4	ENSG00000101489	ENST00000420428.7	1461

**Table 2.0 continued: Coding Sequence (CDS) length of 89 high confidence risk genes associated with ASD due to haploinsufficiency. Highlighted are those genes that exceed rAAV base pair capacity (>/ 3500 base pairs).**

<b>hugoGene</b>	<b>Gene ID</b>	<b>Transcript ID</b>	<b>CDS Length (bp)</b>
PHF12	ENSG00000109118	ENST00000332830.9	3015
TBR1	ENSG00000136535	ENST00000389554.8	2049
PPP2R5D	ENSG00000112640	ENST00000485511.6	1809
TM9SF4	ENSG00000101337	ENST00000398022.7	1929
PHF21A	ENSG00000135365	ENST00000418153.6	2043
PRR12	ENSG00000126464	ENST00000418929.7	6111
SKI	ENSG00000157933	ENST00000378536.5	2187
ASXL3	ENSG00000141431	ENST00000269197.12	6747
SPAST	ENSG00000021574	ENST00000615843	1851
SMARCC2	ENSG00000139613	ENST00000267064.8	3645
TRIP12	ENSG00000153827	ENST00000283943	6123
CREBBP	ENSG00000005339	ENST00000262367	7329
TCF4	ENSG00000196628	ENST00000356073	2322
CACNA1E	ENSG00000198216	ENST00000367570.5	6813
GNAI1	ENSG00000127955	ENST00000649796.2	1065
TCF20	ENSG00000100207	ENST00000677622.1	5883
FOXP2	ENSG00000128573	ENST00000393491	2223
NSD1	ENSG00000165671	ENST00000439151	8091
TCF7L2	ENSG00000148737	ENST00000627217.3	1809
EIF3G	ENSG00000130811	ENST00000253108.9	963
PHF2	ENSG00000025293	ENST00000374012.8	3039
KIAA0232	ENSG00000170871	ENST00000307659.6	4188
VEZF1	ENSG00000136451	ENST00000581208.2	1566
IRF2BPL	ENSG00000119669	ENST00000238647.5	2391
ZMYND8	ENSG00000101040	ENST00000458360.6	3165
RFX3	ENSG00000080298	ENST00000617270.5	2250
SCN1A	ENSG00000144285	ENST00000375405	6030
PPP5C	ENSG00000011485	ENST00000012443.9	1500
GRIA2	ENSG00000120251	ENST00000296526.12	2652
LRRC4C	ENSG00000148948	ENST00000528697.6	1923
CACNA2D3	ENSG00000157445	ENST00000474759.6	3276
NUP155	ENSG00000113569	ENST00000231498.8	4176
KMT2E	ENSG00000005483	ENST00000311117.8	5577
NR3C2	ENSG00000151623	ENST00000358102.8	2955
NACC1	ENSG00000160877	ENST00000292431.5	1584
PTK7	ENSG00000112655	ENST00000230419.9	3213
PPP1R9B	ENSG00000108819	ENST00000612501.2	2454
GABRB2	ENSG00000145864	ENST00000393959.6	1539
HDLBP	ENSG00000115677	ENST00000310931.10	3807
TAOK1	ENSG00000160551	ENST00000261716.8	3006
TEK	ENSG00000120156	ENST00000380036.10	3375
KCNMA1	ENSG00000156113	ENST00000286628.14	3711
CORO1A	ENSG00000102879	ENST00000219150.10	1386
HECTD4	ENSG00000173064	NM_001109662.4	13287
NCOA1	ENSG00000084676	ENST00000348332.8	4326



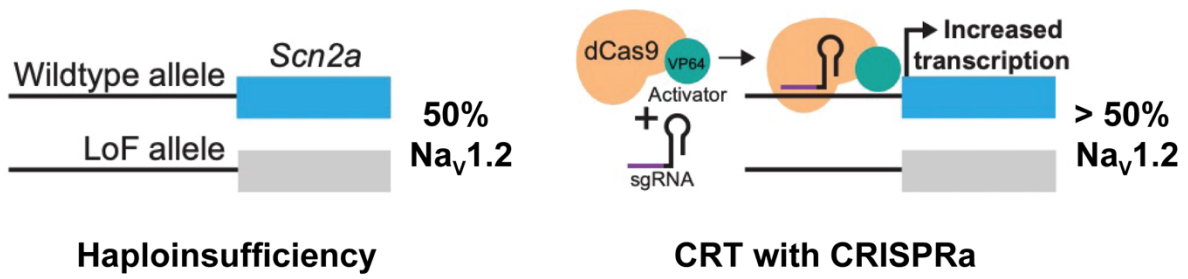


**Figure 1.1: Schematic of *Cis*-regulation therapy using CRISPR activation (CRISPRa) to rescue *Scn2a* haploinsufficiency.**

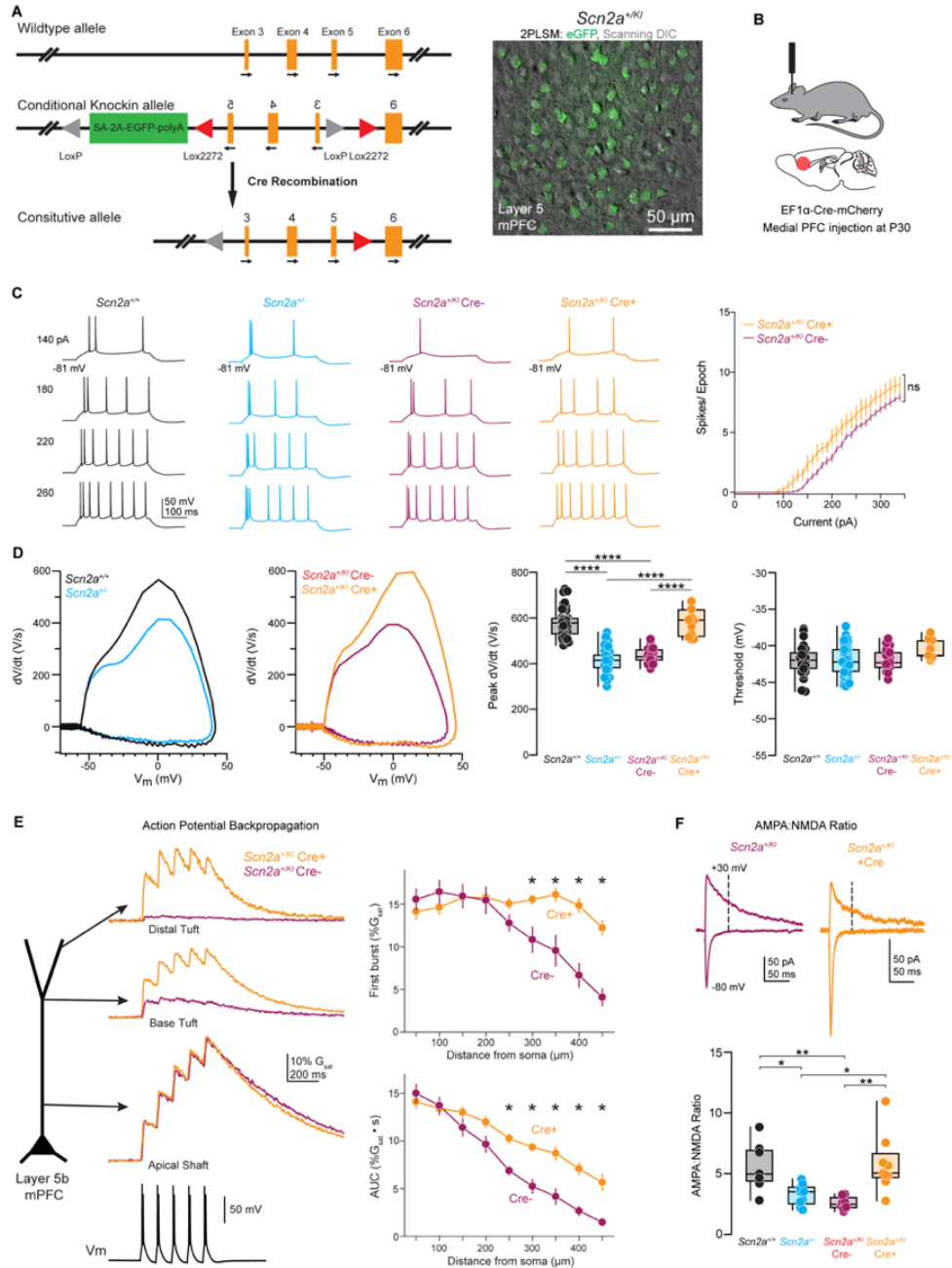


**Figure 2.1: Inducible restoration of two functional *Scn2a* copies in adolescent mice rescues electrophysiological deficits.**

A: Left: *Scn2a*<sup>+/*KI*</sup> inducible recovery mouse model genetic design and allele restoration approach. Right: 2PLSM z-stack of layer 5 of medial prefrontal cortex (mPFC) from coronal brain slice from *Scn2a*<sup>+/*KI*</sup> inducible recovery mouse before Cre injection.

B: Schematic of rAAV-EF1 $\alpha$ -Cre-mCherry injection at P30-40 into the mPFC of *Scn2a*<sup>+/*KI*</sup> inducible recovery mouse.

C: Left: APs generated from current injection in wild type, *Scn2a*<sup>+/-</sup>, *Scn2a*<sup>+/*Kl*</sup> *Cre*<sup>-</sup> and *Scn2a*<sup>+/*Kl*</sup> *Cre*<sup>+</sup> layer 5 pyramidal neurons. Right: Number of APs per 300-ms stimulation epoch across a range of current amplitudes (0-340 pA, 10 pA intervals).

D: Left: Representative phase-plane plots (dV/dt versus voltage) of somatic APs in wild-type, *Scn2a*<sup>+/-</sup>, *Scn2a*<sup>+/*Kl*</sup> *Cre*<sup>-</sup> and *Scn2a*<sup>+/*Kl*</sup> *Cre*<sup>+</sup> neurons. Middle: Peak dV/dt of the first AP evoked by a near-rheo-base current spike train. Right: AP threshold as  $V_m$  when dV/dt measurements first exceed 15 V/s.

E: 2PLSM imaging of bAP evoked Ca transients every 50  $\mu$ m across the apical dendrites of L5 thick-tufted neurons. Calcium transients evoked by bursts of AP doublets.

F: Top: AMPA receptor-mediated and mixed AMPA/NMDA receptor-mediated evoked EPSCs at -80 and +30 mV, respectively. NMDA receptor-mediated component was calculated 50 ms after stimulation (dotted line). Bottom: Quantification of AMPA:NMDA ratio in wild type, *Scn2a*<sup>+/-</sup>, *Scn2a*<sup>+/*Kl*</sup> *Cre*<sup>-</sup> and *Scn2a*<sup>+/*Kl*</sup> *Cre*<sup>+</sup> neurons. \*  $p < 0.01$ , Two-sided Mann-Whitney

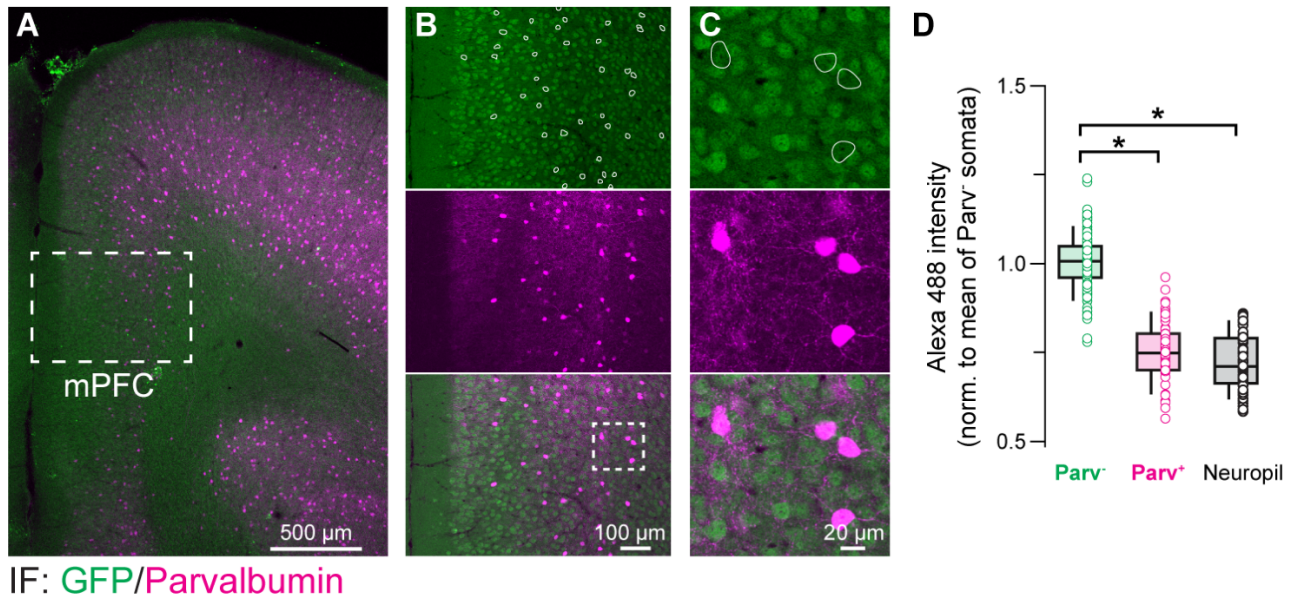


**Figure 2.2: Confocal imaging of neocortical pyramidal neurons in *Scn2a*<sup>+/*Kl*</sup> animals.**

A-C: Coronal brain sections from *Scn2a*<sup>+/*Kl*</sup> mice immunostained with anti-GFP and anti-parvalbumin (PV).

D: Layer 5 excitatory pyramidal cells were GFP+ demonstrating haploinsufficiency of *Scn2a*, distinct from parvalbumin-positive (PV+) GABAergic interneurons.

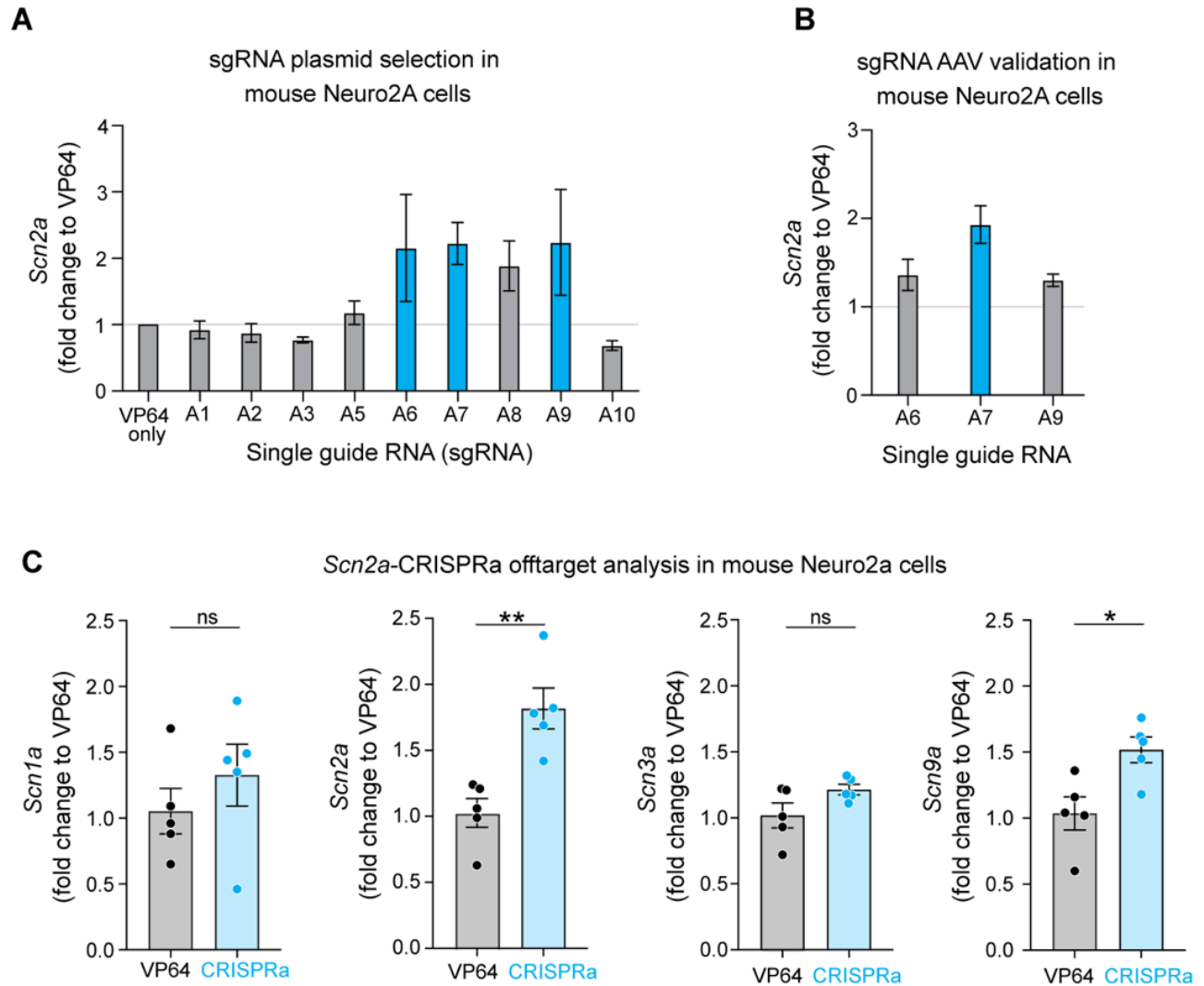


**Figure 2.3: *In vitro* optimization of CRISPRa constructs in mouse Neuroblastoma-2A (Neuro-2A) cells**

A-B: Fold change in *Scn2a* expression in Neuro-2a cells transfected with plasmids (A) or transduced with rAAV-DJ (B) expressing sgRNAs targeting the promoter of mouse *Scn2a* compared to a no sgRNA VP64 only treated control.

C: *In vitro* off-target analysis of transcripts encoding other sodium channels in topologically associated domain (TAD). *Scn7a* excluded due to low endogenous levels of mRNA expression in Neuro-2A cells.

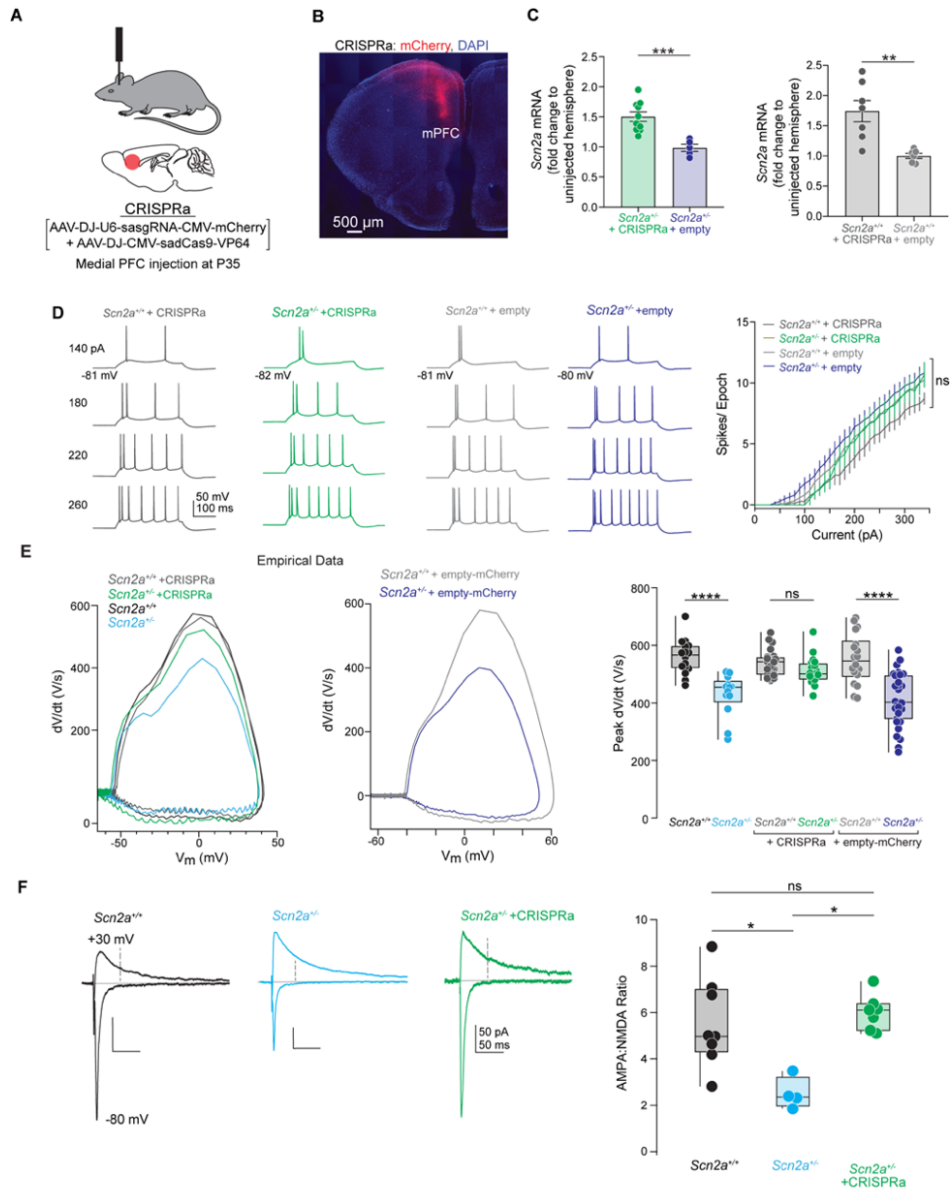


**Figure 2.4: Local administration of *Scn2a*-rAAV-CRISPRa rescues deficits in *Scn2a*<sup>+/-</sup> mice.**

A: Schematic of local injection of *Scn2a*-rAAV-CRISPRa in mPFC.

B: Confocal image of coronal brain section immunostained with antibodies against anti-mCherry and DAPI stain following unilateral injection of *Scn2a*-rAAV-CRISPRa in *Scn2a*<sup>+/-</sup> mice mPFC.

C: *In vivo* *Scn2a* mRNA fold change following local injection of *Scn2a*-rAAV-CRISPRa or *Scn2a*-rAAV-empty in wild type and *Scn2a*<sup>+/-</sup> mice compared to its respective uninjected hemispheres.

D: Left: APs generated from current injection in layer 5 pyramidal neurons of wild type and constitutive *Scn2a*<sup>+/-</sup> mice treated with *Scn2a*-rAAV-CRISPRa or *Scn2a*-rAAV-

empty. Right: Number of APs per 300-ms stimulation epoch across a range of current amplitudes (0-340 pA, 10 pA intervals).

E: Left: Representative phase-plane plots of somatic APs (dV/dt versus voltage) of wild type and constitutive *Scn2a*<sup>+/-</sup> mice treated with *Scn2a*-rAAV-CRISPRa or *Scn2a*-rAAV-empty. Right: Quantification of peak dV/dt.

F: Left: AMPA receptor-mediated and mixed AMPA/NMDA receptor-mediated evoked EPSCs at -80 and +30 mV, respectively. NMDA receptor-mediated component was calculated 50 ms after stimulation (dotted line). Right: Quantification of AMPA:NMDA ratio in wild type, *Scn2a*<sup>+/-</sup> mice and *Scn2a*-rAAV-CRISPRa treated *Scn2a*<sup>+/-</sup> mice.

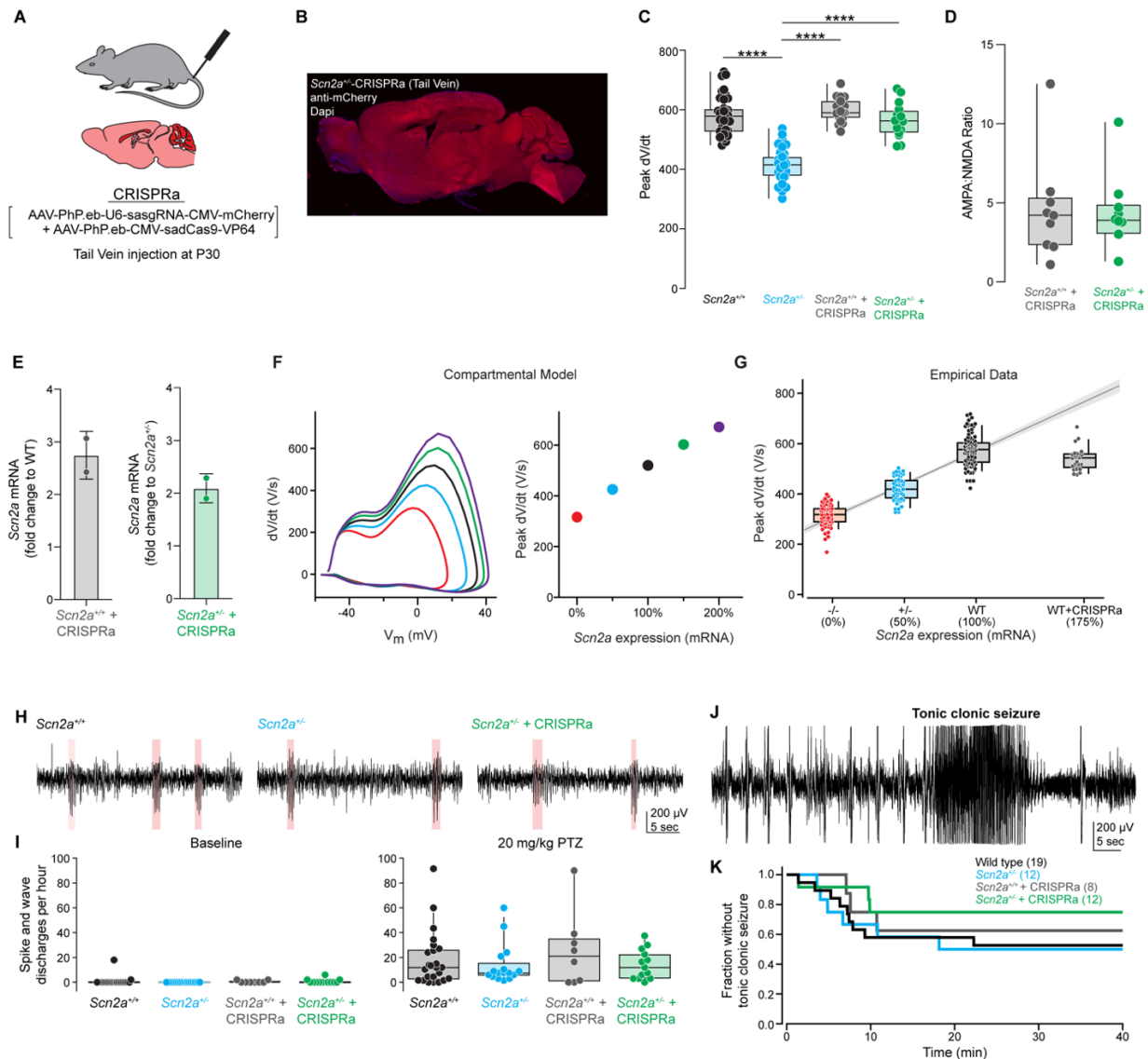


**Figure 2.5: Systemic delivery of CRISPRa does not induce neuronal hyperexcitability.**

A: Schematic of intravenous tail vein delivery of *Scn2a*-rAAV-CRISPRa-PhP.eb.  
 B: Immunofluorescence of mCherry and DAPI staining in sagittal brain sections following intravenous administration of *Scn2a*-rAAV-CRISPRa-PhP.eb in *Scn2a*<sup>+/-</sup> mice.  
 C: Quantification of peak dV/dt of *Scn2a*-rAAV-CRISPRa-PhP.eb treated wild-type, *Scn2a*<sup>+/-</sup> mice and constitutive wild-type and *Scn2a*<sup>+/-</sup> mice.  
 D: Quantification of AMPA:NMDA ratio from *Scn2a*-rAAV-CRISPRa-PhP.eb treated wild-type and *Scn2a*<sup>+/-</sup> mice.  
 E: *In vivo* *Scn2a* mRNA fold change following systemic injection of *Scn2a*-rAAV-CRISPRa-PhP.eb in wild-type and *Scn2a*<sup>+/-</sup> mice.  
 F: Computational modeling of peak dV/dt across varying amounts of *Scn2a* mRNA expression.  
 G: Empirical measurements of peak dV/dt in *Scn2a*-rAAV-CRISPRa treated wild-type mice versus untreated wild type, *Scn2a*<sup>+/-</sup>, and *Scn2a*<sup>-/-</sup> mice.



H: Baseline recordings of spike and wave discharges in wild type, *Scn2a*<sup>+/-</sup> and *Scn2a*-rAAV-CRISPRa-PhP.eb treated wild type and *Scn2a*<sup>+/-</sup> mice.

I: SWD discharges at baseline and low dose (20 mg/kg) of pentylenetetrazole (PTZ) challenge.

J: Induction of tonic clonic seizures following high dose (50 mg/kg) treatment of PTZ.

K: Survival curves following high dose (50 mg/kg) treatment of PTZ.

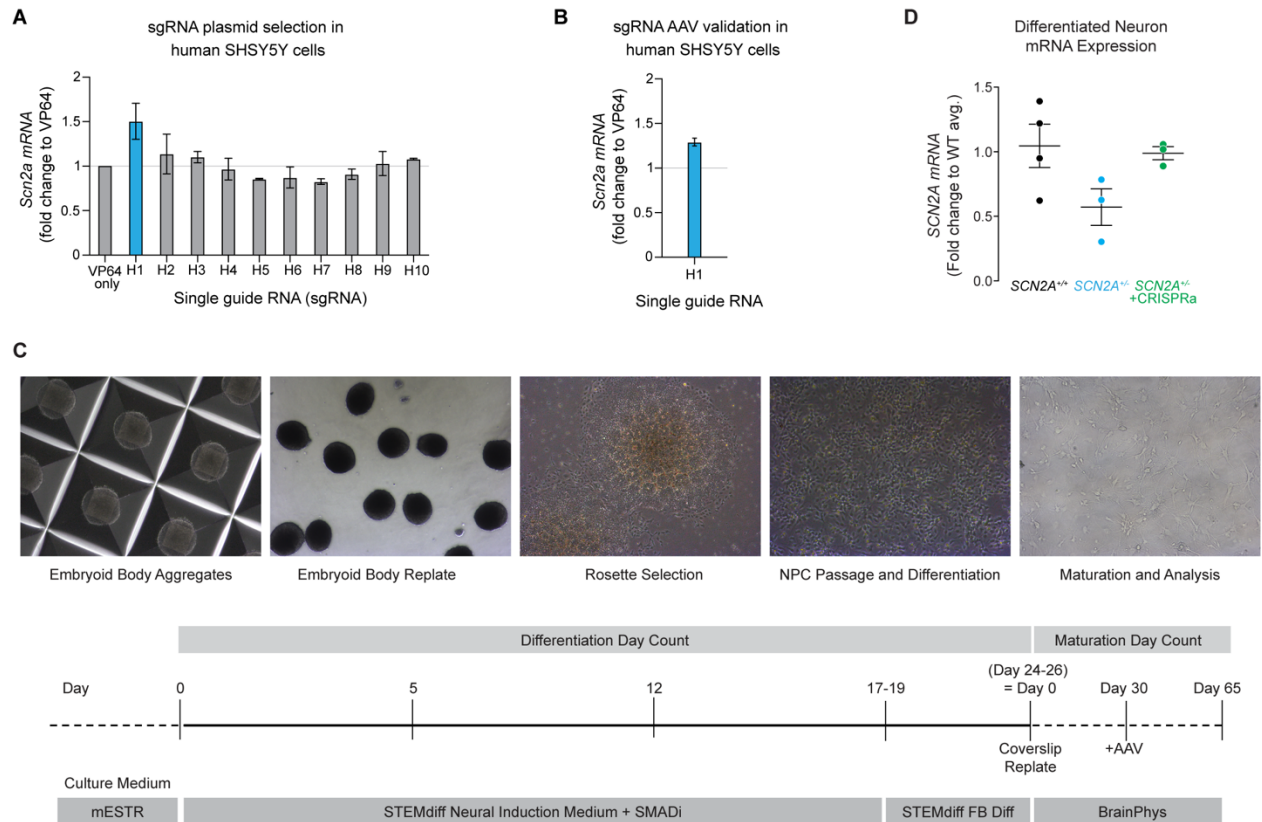


**Figure 2.6: *in vitro* optimization of mouse CRISPRa constructs in SH-SY5Y cells**  
 S4A-S4B: *in vitro* sgRNA screening for human *SCN2A* constructs in SH-SY5Y cells in plasmid and rAAV-DJ.  
 S4C: hESC differentiated neuron strategy and schematic.  
 S4D: *in vitro* *SCN2A* mRNA expression in wild-type, *SCN2A*<sup>+/-</sup> and *SCN2A*-rAAV-CRISPRa treated heterozygous neurons compared to wild-type expression average.

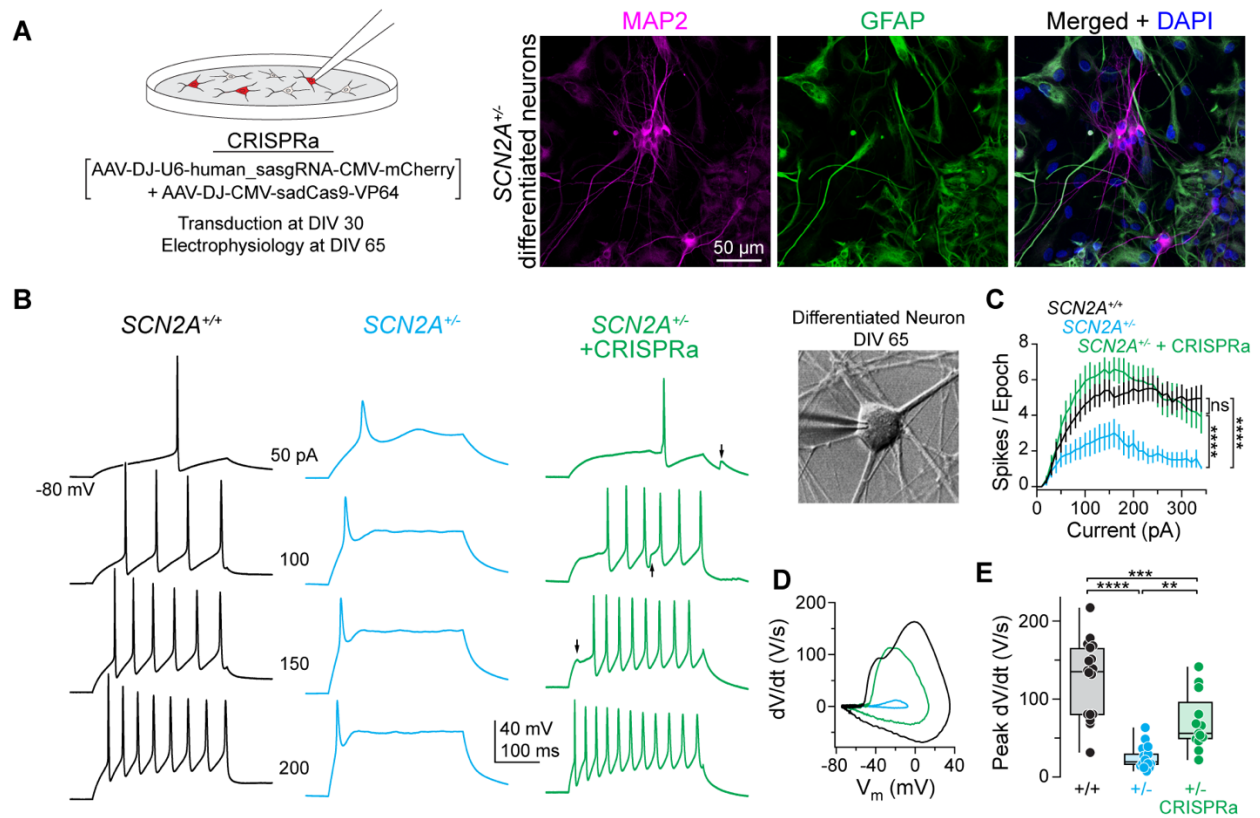


**Figure 2.7: SCN2A-rAAV-CRISPRa treatment in human differentiated neuronal cells.**

A: Schematic of CRISPRa treatment in differentiated neurons and immunofluorescence of SCN2A<sup>+/-</sup> differentiated neurons at DIV 65 immunostaining with antibodies against MAP2, GFAP and DAPI.

B-C: APs generated from current injections of differentiated neurons at DIV 65 from wild-type, SCN2A<sup>+/-</sup>, and SCN2A-rAAV-CRISPRa treated SCN2A<sup>+/-</sup> differentiated neurons.

D-E: Representative phase-plane plots and quantification of peak dV/dt in wild type, SCN2A<sup>+/-</sup>, and SCN2A-rAAV-CRISPRa treated SCN2A<sup>+/-</sup> differentiated neurons.

**Table 2.8: Primer and sgRNA sequences used in this dissertation.**

Primers	Forward	Reverse
qPCR-Mouse_Scn2a	ATTTTCGGCTCATTCTTCACACT	GGGCGAGGTATCGGTTTTTGT
qPCR-Mouse_Bactin	GACGATGCTCCCCGGGCTGTATTC	TCTCTTGCTCTGGGCCTCGTCACC
qPCR-sadCas9-VP64	ATCACCCCCCACCAGATCAAGC	GTCCTTGTCGTACAGGCCGTTCA
qPCR-Human_SCN2A	CGCTTCTTTACCAGGGAATCC	TCCTGTTGGGTCTCTTAGCTTT
qPCR-Human_Bactin	CATGTACGTTGCTATCCAGGC	CTCCTTAATGTCACGCACGAT
genotyping-Mouse_Scn2a	TGCGAGGAGCTAAACAGTGATTAAG	GGCTCCATTCCCTTATCAGACCTACCC

tested sgRNA	
mouse_Scn2a	sgRNA sequence
A1	ACAGAATCAGTAACGCACTGT
A2	CGGGTAAGCCAAGTTTAGTCA
A3	AAGCACTTGCCCTCACATAAAT
A5	CTAGGTCATAGAAAGGAAACC
A6	TTTATTGGACCCCAGATATTC
A7	AGAAAATTAACCTTAGTGCATA
A8	AAGCCGCCAGGGACCCGAGCA
A9	TATACTGCCACTAGAGGGCT
A10	GACCCTCCTCCGGGCTCCACC
human_SCN2A	sgRNA sequence
H1	TGCTGACTGCTACATAGCCAA
H2	GTGCTGACTGCTACATAGCCA
H3	CTGCTACATAGCCAAAGGAAC
H4	GCTCCATCTCCTGGTCAAAAAG
H5	CAGCCCATAATTCCACTCTAT
H6	AGTAGTTGATTTCAAATAGAG
H7	ATTAAAGTAGTTGATTTCAAAA
H8	GATTTCAAATAGAGTGGAAAT
H9	AAGTAGTTGATTTCAAATAGA
H10	AGCTCCATCTCCTGGTCAAAA

## **Chapter 3: Concluding Remarks**

### 3.1: Overview

Autism spectrum disorder (ASD) is a common neurodevelopmental disorder (NDD) affecting 1 in 54 school-aged children in the US (Maenner et al., 2020 & Elsabbagh et al., 2012). Recent advances in gene discovery have facilitated the identification of 102 high confidence ASD *de novo* risk genes. The majority of these risk genes (N=89) are either known or predicted to cause ASD due to haploinsufficiency, where the mRNA/protein levels from the residual gene copy are insufficient (Satterstrom et al., 2020). Delivering functional gene copies via gene therapy could potentially restore transcriptional balance and rectify deficits in haploinsufficient diseases. Gene therapy primarily relies on using recombinant adeno-associated virus (rAAV) for transgene delivery due to its limited pathogenicity and long-term transgene expression (Wang et al., 2019). However, rAAV has relatively limited packaging capacity (4,700 base pairs optimal packaging capacity minus ~1,700 base pairs needed for transgene expression). Examination of the coding sequence (CDS) length of the 89 aforementioned haploinsufficient ASD risk genes shows that 40 exceed rAAV vector capacity (Table 2.0), excluding them from traditional gene replacement therapy approaches (Howe et al., 2021).

Here, we tested whether *Cis*-Regulation therapy (CRT), a novel therapeutic approach that uses nuclease deficient gene-editing systems, such as a dead Cas9 (dCas9), fused to a transcriptional modulator/s to change the activity of a gene's regulatory elements for therapeutic benefit (Matharu & Ahituv, 2020), could be a viable approach for treating ASD-associated haploinsufficiency regardless of gene size. For our proof-of-concept,

we utilized ASD-associated haploinsufficiency of the sodium voltage-gated channel alpha subunit 2 (*SCN2A*), a gene with a six kilobase-long CDS (Howe et al., 2021). Mutations that lead to *SCN2A* loss-of-function (LoF) are one of the most significant genetically defined subsets of ASD, second to Fragile X (Ben-Shalom et al., 2017) contributing to over 10,000 cases of ASD in the US per year (0.3% of all ASD cases) (Sanders et al., 2015; Ben-Shalom et al., 2017). In addition to ASD, individuals frequently have severe intellectual disability and poor developmental outcomes (Sanders et al., 2015; Sanders et al., 2018; Ben-Shalom et al., 2017).

*SCN2A* encodes the neuronal voltage-gated sodium channel, Nav<sub>v</sub>1.2, which is expressed in the axon initial segment (AIS) of excitatory neurons. Early in development (first year of life in humans and one week in mice) Nav<sub>v</sub>1.2 plays an essential role as the primary Nav<sub>v</sub> responsible for in action potential (AP) firing. Later in development Nav<sub>v</sub>1.2 takes on the role as an AP signal booster, which promotes synaptic integration and dendritic excitability (Spratt 2019 and 2021). These traits are readily measured via electrophysiology, which it provides an efficient and quantifiable testbed for CRT-based interventions. Here, we tested CRISPRa-based CRT in both mouse models and in *SCN2A* heterozygous neurons differentiated from human embryonic stem cells (hESCs) (Lu et al., 2019), and demonstrate that this approach can rescue excitability deficits without inducing hyperexcitability when administered at adolescent stages. Combined, our work showcases a potential therapeutic approach that could be applied to numerous ASD-associated genes and suggests that rescue later in life could ameliorate electrophysiological phenotypes associated with *Scn2a* haploinsufficiency.

### 3.2: Towards a Therapy and Future Directions

Neurodevelopmental disorders (NDD) were traditionally thought to be a static disorder from birth, with interventions and treatment assumed to be most beneficial within fixed critical time windows of brain development, usually before the onset of the disorder (Marín, 2016). However, brain development and the integration of neural circuits is a dynamic process that spans multiple decades of life and are now thought to be more plastic with potential space for therapeutic intervention later in life (Levy, 2020). Both our genetic and rAAV-CRISPRa adolescent rescue of electrophysiological deficits in *Scn2a* heterozygous mice add to a growing body of literature that suggests that our understanding of the critical window to treat NDD is more dynamic than previously thought. For example, the use of antisense oligonucleotides (ASO) to treat Angelman Syndrome (AS) later in life (4-17 years of age), has been shown to be an effective therapeutic strategy, with preliminary results from a Phase I/II clinical trial showing improvements in communication and motor skills and a reduction in epileptiform discharges (Schmid et al., 2021). Further development of precision therapies that target genes associated with NDD will likely increase our understanding of neuronal plasticity and what is the critical window during which these conditions can be treated.

Pharmacological interventions targeting sodium channelopathies have largely been unsuccessful, primarily due to off-target effect concerns. There are nine sodium channels in the human genome with similar protein structures, but each with different essential functions in the skeletal, cardiac, central and peripheral nervous systems



(Deuis et al., 2017). Selective sodium channel activators that might be used to compensate for LoF mutations are extremely difficult drug targets due to off-target toxicity, which is of particular concern considering the central functions that these channels provide (Waszkielewicz et al., 2013). CRT could overcome this off-target issue as it targets endogenous DNA sequences that regulate these gene expression patterns. While there is certainly a concern of CRISPR off-target binding, our qPCR results show no apparent off-target effects with respect to altered expression of other sodium channel transcripts, and future development of improved nuclease deficient gene-editing systems with increased binding specificities (Matharu & Ahituv, 2020) could also improve and ameliorate this concern.

In the case of sodium channel haploinsufficiency, CRT also overcomes two of the main limitations of traditional gene replacement therapy, rAAV vector capacity and ectopic expression. Sodium channels are large genes whose cDNA is above the rAAV payload capacity. CRT overcomes this by packaging CRISPRa components that target the gene's regulatory elements to upregulate mRNA its expression. In addition, results from a transgenic-based CRISPRa approach suggest that upregulation occurs only in the tissue/cell type where the targeted regulatory element is active (Matharu et al., 2019), providing additional specificity to the rAAV serotype or promoter used to drive expression. An additional advantage is that CRT uses a nuclease-deficient DNA targeting molecule that does not edit the DNA, and thus off-target effects will not lead to 'DNA scars'. While the use of a CRISPR-based CRT approach could lead to immunogenicity due to the dCas9, there are many efforts underway to engineer Cas

proteins with reduced immunogenicity by epitope masking (Mehta and Merkel, 2019 & Ferdosi et al., 2019) or use of alternate Cas proteins, such as those from non-pathogenic bacteria that have not been exposed to humans (Matharu & Ahituv, 2020). Alternatively, other DNA targeting molecules, like zinc fingers or Transcription Activator-Like Effector Nucleases (TALENs) that should be less immunogenic and smaller in size (Gaj et al., 2016) could be used instead.

This study used rAAV as the delivery vehicle for our CRT constructs. Viral vectors, particularly rAAVs, have long been the gold standard for gene therapies and are used in hundreds of clinical trials, largely due to their limited pathogenicity and long term episomal transgene expression. However, there are limitations to rAAVs that impede the treatment of gene-based therapies. One of the main limitations of rAAVs is its vector capacity. While CRT circumvents the need to package the entire transgene into the rAAV, which thereby increases the number of genes that can be modulated for therapeutic effect, rAAV vector capacity can still be optimized. One way to optimize vector capacity is to utilize other proteins in the CRISPR toolbox, such as smaller nuclease-free Cas species like Cas $\Phi$  or Cas12a, which are both significantly smaller than Cas9 and can still efficiently target and edit human cells (Pausch et al., 2020).

An additional limitation to viral delivery vehicles like rAAV is their pathogenicity in the context of repeat dosing. In this study we showed therapeutic efficacy from a single rAAV injection when targeting neurons. However, targeting other cell types that are not post-mitotic, which may divide out the episomal transgene, could require multiple

treatments to maintain therapeutic efficacy. Neutralizing antibodies (Nabs), which target rAAV capsids, can not only reduce cell transduction efficacy but might also cause an immunogenic reaction to repeat dosings of rAAV treatment and thereby hinder its use as a therapeutic.

Alternative delivery vehicles may overcome the limitations of rAAV Nab immunogenicity. Non-viral delivery particles like synthetic nanoparticles have been developed as alternatives to viral vectors, and hundreds are being tested in clinical trials. Synthetic nanoparticles made from lipid, gold and polymers have been extensively studied. They can package larger genetic payloads and are amenable to repeat dosing with Nab interference (Anselmo and Mitragotri, 2019). Gold based nanoparticle delivery of CRISPR particles into the brain has been shown to be effective in ameliorating atypical behaviors in mouse Fragile X models, which sets precedence for its benefit in the treatment of NDDs (Lee et al., 2018). However, stable transgene expression is not currently achievable using these particles and falls short when compared to stable episomal expression from rAAVs.

Here we showed how CRT using CRISPRa was able to rebalance mRNA expression to physiologically relevant levels, thereby ameliorating electrophysiological deficits associated with *SCN2A* haploinsufficiency. Other groups have applied a similar therapeutic strategy using CRISPRa to rectify haploinsufficiency in Dravet Syndrome, which is caused by LoF mutations in *SCN1A* (Colasante et al., 2020; Ricci et al., 2021). Beyond activating mRNA expression, others have applied the use of CRISPR inhibition

(CRISPRi) as an epigenetic therapy to downregulate the expression of other sodium channels, like *SCN9A*, to suppress chronic pain *in vivo* (Moreno et al., 2021). Together these applications point to the therapeutic effect of targeting single genes associated with dosage imbalance using dCas9 based therapeutics. Future development of CRT could be used to target disorders that are caused by mutations in multiple genes by multiplexing sgRNAs. This might be advantageous in treating large chromosomal deletions and disorders caused by variations in copy number, such as deletions and duplications of variants like 22q11 and 16p11, both of which are highly associated with neurodevelopmental and neuropsychiatric disorders.

It is currently vital to make sure that the treated mutation causes a non-functional transcript, as our current approach upregulates both alleles. Future developments that take advantage of allele-specific nucleotide variation to upregulate specific alleles could potentially be used (Wu et al., 2019). Further development of CRT using CRISPRa/i could be through technological developments in allele specificity. For example, in the treatment of dominant negative mutations, such as *SCN2A* GoF mutations, reducing mRNA expression from the pathogenic allele with CRISPRi or even CRISPR deletion could ameliorate the associated epileptic phenotypes. However, simply reducing mRNA expression from the pathogenic GoF allele would still result in a haploinsufficient condition, as mRNA expression will be reduced by 50%. The ability to both down and upregulate gene expression based on allele specificity will be essential in treating dosage conditions that require more nuanced levels of gene expression beyond gene augmentation like dominant negative mutations. Other molecular medicines such as

antisense oligonucleotides, short-interfering RNAs (siRNAs) and TALENs have shown success in allele specific interventions, which suggest potential for future success in the development of allele specific sgRNA (Fink et al., 2016). Current models of allele specific sgRNA technology utilizes gene mutations or single nucleotide polymorphisms (SNPs) that either creates a novel protospacer adjacent motif (PAM) site at or around existing PAM sites to provide discrepancy between the two alleles.

### 3.3: Conclusion

Our ability to rescue electrophysiological deficits in *SCN2A*<sup>+/-</sup> hESC differentiated excitatory neurons, further showcases the translational potential of this approach. However, numerous hurdles remain requiring many experiments to be conducted to translate this treatment into the clinic. Many individual aspects of the approach will need to be optimized, including safety assessments of rAAV components, off-target effects, the use of non-human primates to assess efficient delivery, degree of upregulation, cytotoxicity, immunogenicity and other effects. In addition, it will be vital to confirm that the treated mutation causes a non-functional transcript, as our current approach upregulates both alleles. Further developments that take advantage of allele-specific nucleotide variation to upregulate specific alleles could be used in the future (Wu et al., 2019).

In summary, this study shows how CRT using CRISPRa can rescue a major class of mutations in one of the most significant ASD risk genes. CRT is a customizable platform technology that can modify mutations in the DNA without directly editing the genome, and can be tailored to rescue other haploinsufficient disorders, including other NDD. The application of this therapeutic approach leverages a growing understanding of the biological mechanisms that make up the autism spectrum and offers biologically salient targets to modify complex behaviorally defined conditions like ASD.

## References

## References

- Anselmo, Aaron C., and Samir Mitragotri. "Nanoparticles in the Clinic: An Update." *Bioengineering & Translational Medicine* 4, no. 3 (September 2019): e10143.
- Ben-Shalom, Roy, Caroline M. Keeshen, Kiara N. Berrios, Joon Y. An, Stephan J. Sanders, and Kevin J. Bender. "Opposing Effects on NaV1.2 Function Underlie Differences Between SCN2A Variants Observed in Individuals With Autism Spectrum Disorder or Infantile Seizures." *Biological Psychiatry* 82, no. 3 (August 1, 2017): 224–32.
- Bender, K.J., and Trussell, L.O. (2012). The physiology of the axon initial segment. *Annu. Rev. Neurosci.* 35, 249–265.
- Bender, Kevin J., and Laurence O. Trussell. "Axon Initial Segment Ca<sup>2+</sup> Channels Influence Action Potential Generation and Timing." *Neuron* 61, no. 2 (January 29, 2009): 259–71.
- Boiko, T., Van Wart, A., Caldwell, J.H., Levinson, S.R., Trimmer, J.S., and Matthews, G. (2003). Functional specialization of the axon initial segment by isoform-specific sodium channel targeting. *J. Neurosci.* 23, 2306–2313.
- Chater, Thomas E., and Yukiko Goda. "The Role of AMPA Receptors in Postsynaptic Mechanisms of Synaptic Plasticity." *Frontiers in Cellular Neuroscience* 8 (November 27, 2014).
- Chavez, Alejandro, Marcelle Tuttle, Benjamin W Pruitt, Ben Ewen-Campen, Raj Chari,



- Dmitry Ter-Ovanesyan, Sabina J Haque, et al. "Comparative Analysis of Cas9 Activators Across Multiple Species." *Nature Methods* 13, no. 7 (July 2016): 563–67
- Colasante, Gaia, Gabriele Lignani, Simone Brusco, Claudia Di Bernardino, Jenna Carpenter, Serena Giannelli, Nicholas Valassina, et al. "DCas9-Based Scn1a Gene Activation Restores Inhibitory Interneuron Excitability and Attenuates Seizures in Dravet Syndrome Mice." *Molecular Therapy: The Journal of the American Society of Gene Therapy* 28, no. 1 (January 8, 2020): 235–53.
- Deuis, Jennifer R., Lucie S. Dvorakova, and Irina Vetter. "Methods Used to Evaluate Pain Behaviors in Rodents." *Frontiers in Molecular Neuroscience* 10 (2017): 284.
- Deverman, Benjamin E., Piers L. Pravdo, Bryan P. Simpson, Sripriya Ravindra Kumar, Ken Y. Chan, Abhik Banerjee, Wei-Li Wu, et al. "Cre-Dependent Selection Yields AAV Variants for Widespread Gene Transfer to the Adult Brain." *Nature Biotechnology* 34, no. 2 (February 2016): 204–9.
- Elsabbagh, Mayada, Gauri Divan, Yun-Joo Koh, Young Shin Kim, Shuaib Kauchali, Carlos Marcín, Cecilia Montiel-Nava, et al. "Global Prevalence of Autism and Other Pervasive Developmental Disorders." *Autism Research* 5, no. 3 (June 2012): 160–79.
- Ferdosi, Shayesteh R., Radwa Ewaisha, Farzaneh Moghadam, Sri Krishna, Jin G. Park, Mo R. Ebrahimkhani, Samira Kiani, and Karen S. Anderson. "Multifunctional CRISPR-Cas9 with Engineered Immunosilenced Human T Cell Epitopes." *Nature Communications* 10, no. 1 (December 2019): 1842.
- Fink, Kyle D., Peter Deng, Josh Gutierrez, Joseph S. Anderson, Audrey Torrest, Anvita

- Komarla, Stefanos Kalomoiris, et al. "Allele-Specific Reduction of the Mutant Huntingtin Allele Using Transcription Activator-Like Effectors in Human Huntington's Disease Fibroblasts." *Cell Transplantation* 25, no. 4 (2016): 677–86.
- Gaj, Thomas, Shannon J. Sirk, Sai-lan Shui, and Jia Liu. "Genome-Editing Technologies: Principles and Applications." *Cold Spring Harbor Perspectives in Biology* 8, no. 12 (December 2016): a023754.
- Gazina, E.V., Leaw, B.T.W., Richards, K.L., Wimmer, V.C., Kim, T.H., Aumann, T.D., Featherby, T.J., Churilov, L., Hammond, V.E., Reid, C.A., et al. (2015). "Neonatal" Nav1.2 reduces neuronal excitability and affects seizure susceptibility and behaviour. *Hum. Mol. Genet.* 24, 1457–1468.
- Haery, Leila, Benjamin E. Deverman, Katherine S. Matho, Ali Cetin, Kenton Woodard, Connie Cepko, Karen I. Guerin, et al. "Adeno-Associated Virus Technologies and Methods for Targeted Neuronal Manipulation." *Frontiers in Neuroanatomy* 0 (2019).
- Howe, Kevin L, Premanand Achuthan, James Allen, Jamie Allen, Jorge Alvarez-Jarreta, M Ridwan Amode, Irina M Armean, et al. "Ensembl 2021." *Nucleic Acids Research* 49, no. D1 (January 8, 2021): D884–91.
- Hyman, Susan L., Susan E. Levy, Scott M. Myers, and Section on Developmental and Behavioral Pediatrics Council on Children with Disabilities. "Identification, Evaluation, and Management of Children With Autism Spectrum Disorder." *Pediatrics* 145, no. 1 (January 1, 2020).
- Kole, M.H.P., and Stuart, G.J. (2012). Signal Processing in the Axon Initial Segment. *Neuron* 73, 235–247.

- Kole, M.H.P., Ilschner, S.U., Kampa, B.M., Williams, S.R., Ruben, P.C., and Stuart, G.J. (2008). Action potential generation requires a high sodium channel density in the axon initial segment. *Nat. Neurosci.* 11, 178–186.
- Lee, Bumwhae, Kunwoo Lee, Shree Panda, Rodrigo Gonzales-Rojas, Anthony Chong, Vladislav Bugay, Hyo Min Park, Robert Brenner, Niren Murthy, and Hye Young Lee. “Nanoparticle Delivery of CRISPR into the Brain Rescues a Mouse Model of Fragile X Syndrome from Exaggerated Repetitive Behaviours.” *Nature Biomedical Engineering* 2, no. 7 (July 2018): 497–507.
- Levy, Gilad, and Boaz Barak. “Postnatal Therapeutic Approaches in Genetic Neurodevelopmental Disorders.” *Neural Regeneration Research* 16, no. 3 (2021): 414.
- Lu, Congyi, Xi Shi, Andrew Allen, David Baez-Nieto, Alexandria Nikish, Neville E. Sanjana, and Jen Q. Pan. “Overexpression of NEUROG2 and NEUROG1 in Human Embryonic Stem Cells Produces a Network of Excitatory and Inhibitory Neurons.” *The FASEB Journal* 33, no. 4 (April 2019): 5287–99.
- Maenner, M. J. “Prevalence of Autism Spectrum Disorder Among Children Aged 8 Years — Autism and Developmental Disabilities Monitoring Network, 11 Sites, United States, 2016.” *MMWR. Surveillance Summaries* 69 (2020).
- Marín, Oscar. “Developmental Timing and Critical Windows for the Treatment of Psychiatric Disorders.” *Nature Medicine* 22, no. 11 (November 2016): 1229–38.
- Markram, Henry, Eilif Muller, Srikanth Ramaswamy, Michael W. Reimann, Marwan Abdallah, Carlos Aguado Sanchez, Anastasia Ailamaki, et al. “Reconstruction and Simulation of Neocortical Microcircuitry.” *Cell* 163, no. 2 (October 8, 2015):

456–92.

Matharu, Navneet, and Nadav Ahituv. “Modulating Gene Regulation to Treat Genetic Disorders.” *Nature Reviews Drug Discovery* 19, no. 11 (November 2020): 757–75.

Matharu, Navneet, Sawitree Rattanasopha, Serena Tamura, Lenka Maliskova, Yi Wang, Adelaide Bernard, Aaron Hardin, Walter L. Eckalbar, Christian Vaisse, and Nadav Ahituv. “CRISPR-Mediated Activation of a Promoter or Enhancer Rescues Obesity Caused by Haploinsufficiency.” *Science* 363, no. 6424 (January 18, 2019): eaau0629.

Mehta, Aditi, and Olivia M. Merkel. “Immunogenicity of Cas9 Protein.” *Journal of Pharmaceutical Sciences* 109, no. 1 (January 1, 2020): 62–67.

Mishra, V., Karumuri, B.K., Gautier, N.M., Liu, R., Hutson, T.N., Vanhoof-Villalba, S.L., Vlachos, I., Iasemidis, L., and Glasscock, E. (2017). Scn2a deletion improves survival and brain-heart dynamics in the Kcna1-null mouse model of sudden unexpected death in epilepsy (SUDEP). *Hum. Mol. Genet.* 26, 2091–2103.

Miyamoto, Hiroyuki, Tetsuya Tatsukawa, Atsushi Shimohata, Tetsushi Yamagata, Toshimitsu Suzuki, Kenji Amano, Emi Mazaki, et al. “Impaired Cortico-Striatal Excitatory Transmission Triggers Epilepsy.” *Nature Communications* 10, no. 1 (April 23, 2019): 1917

Moreno, Ana M., Fernando Alemán, Glaucilene F. Catroli, Matthew Hunt, Michael Hu, Amir Dailamy, Andrew Pla, et al. “Long-Lasting Analgesia via Targeted in Situ Repression of NaV1.7 in Mice.” *Science Translational Medicine* 13, no. 584 (March 10, 2021).

- Osorio, Nancy, Gisèle Alcaraz, Françoise Padilla, François Couraud, Patrick Delmas, and Marcel Crest. "Differential Targeting and Functional Specialization of Sodium Channels in Cultured Cerebellar Granule Cells." *The Journal of Physiology* 569, no. 3 (2005): 801–16.
- Pausch, Patrick, Basem Al-Shayeb, Ezra Bisom-Rapp, Connor A. Tsuchida, Zheng Li, Brady F. Cress, Gavin J. Knott, Steven E. Jacobsen, Jillian F. Banfield, and Jennifer A. Doudna. "CRISPR-Cas $\Phi$  from Huge Phages Is a Hypercompact Genome Editor." *Science* 369, no. 6501 (July 17, 2020): 333–37.
- Planells-Cases, R., Caprini, M., Zhang, J., Rockenstein, E.M., Rivera, R.R., Murre, C., Masliah, E., and Montal, M. (2000). Neuronal Death and Perinatal Lethality in Voltage-Gated Sodium Channel  $\alpha$ II-Deficient Mice. *Biophys. J.* 78, 2878–2891.
- Reynolds, Claire, Mary D. King, and Kathleen M. Gorman. "The Phenotypic Spectrum of SCN2A- Related Epilepsy." *European Journal of Paediatric Neurology* 24 (January 2020): 117–22.
- Ricci, Raffaele, and Gaia Colasante. "CRISPR/DCas9 as a Therapeutic Approach for Neurodevelopmental Disorders: Innovations and Limitations Compared to Traditional Strategies." *Developmental Neuroscience* 43, no. 3–4 (2021): 253–61.
- Sanders, S.J., He, X., Willsey, A.J., Ercan-Sencicek, A.G., Samocha, K.E., Cicek, A.E., Murtha, M.T., Bal, V.H., Bishop, S.L., Dong, S., et al. (2015). Insights into Autism Spectrum Disorder Genomic Architecture and Biology from 71 Risk Loci. *Neuron* 87, 1215–1233.
- Sanders, Stephan J., Arthur J. Campbell, Jeffrey R. Cottrell, Rikke S. Moller, Florence

- F. Wagner, Angie L. Auldridge, Raphael A. Bernier, et al. "Progress in Understanding and Treating SCN2A-Mediated Disorders." *Trends in Neurosciences* 41, no. 7 (July 2018): 442–56.
- Satterstrom, F. Kyle, Jack A. Kosmicki, Jiebiao Wang, Michael S. Breen, Silvia De Rubeis, Joon-Yong An, Minshi Peng, et al. "Large-Scale Exome Sequencing Study Implicates Both Developmental and Functional Changes in the Neurobiology of Autism." *Cell* 180, no. 3 (February 6, 2020): 568-584.e23.
- Schmid, Ralf S., Xuefeng Deng, Priyalakshmi Panikker, Msema Msackyi, Camilo Breton, and James M. Wilson. "CRISPR/Cas9 Directed to the Ube3a Antisense Transcript Improves Angelman Syndrome Phenotype in Mice." *The Journal of Clinical Investigation* 131, no. 5 (n.d.): e142574.
- Shin, W., Kweon, H., Kang, R., Kim, D., Kim, K., Kang, M., Kim, S.Y., Hwang, S.N., Kim, J.Y., Yang, E., et al. (2019). Scn2a Haploinsufficiency in Mice Suppresses Hippocampal Neuronal Excitability, Excitatory Synaptic Drive, and Long-Term Potentiation, and Spatial Learning and Memory. *Front. Mol. Neurosci.* 12, 145
- Spratt, Perry W. E., Roy Ben-Shalom, Atehsa Sahagun, Caroline M. Keeshen, Stephan J. Sanders, and Kevin J. Bender. "Paradoxical Hyperexcitability from NaV1.2 Sodium Channel Loss in Neocortical Pyramidal Cells." *BioRxiv*, February 2, 2021, 2021.02.02.429423.
- Spratt, Perry W.E., Roy Ben-Shalom, Caroline M. Keeshen, Kenneth J. Burke, Rebecca L. Clarkson, Stephan J. Sanders, and Kevin J. Bender. "The Autism-Associated Gene Scn2a Contributes to Dendritic Excitability and Synaptic Function in the Prefrontal Cortex." *Neuron* 103, no. 4 (August 2019): 673-685.e5.

Van Erum, Jan, Debby Van Dam, and Peter Paul De Deyn. "PTZ-Induced Seizures in Mice Require a Revised Racine Scale." *Epilepsy & Behavior: E&B* 95 (June 2019): 51–55.

Wang, Dan, Phillip W. L. Tai, and Guangping Gao. "Adeno-Associated Virus Vector as a Platform for Gene Therapy Delivery." *Nature Reviews. Drug Discovery* 18, no. 5 (May 2019): 358–78.

Waszkielewicz, A.M, A Gunia, N Szkaradek, K Słoczyńska, S Krupińska, and H Marona. "Ion Channels as Drug Targets in Central Nervous System Disorders." *Current Medicinal Chemistry* 20, no. 10 (April 2013): 1241–85.

Wu, Junjiao, Beisha Tang, and Yu Tang. "Allele-Specific Genome Targeting in the Development of Precision Medicine." *Theranostics* 10, no. 7 (February 10, 2020): 3118–37.

Yasuda, R., Nimchinsky, E.A., Scheuss, V., Pologruto, T.A., Oertner, T.G., Sabatini, B.L., and Svoboda, K. (2004). Imaging Calcium Concentration Dynamics in Small Neuronal Compartments. *Sci. Signal.* 2004, pl5-pl5.

## Publishing Agreement

It is the policy of the University to encourage open access and broad distribution of all theses, dissertations, and manuscripts. The Graduate Division will facilitate the distribution of UCSF theses, dissertations, and manuscripts to the UCSF Library for open access and distribution. UCSF will make such theses, dissertations, and manuscripts accessible to the public and will take reasonable steps to preserve these works in perpetuity.

I hereby grant the non-exclusive, perpetual right to The Regents of the University of California to reproduce, publicly display, distribute, preserve, and publish copies of my thesis, dissertation, or manuscript in any form or media, now existing or later derived, including access online for teaching, research, and public service purposes.

DocuSigned by:

*Serena Tamura*

F7C0D1143EBE432...

Author Signature

12/8/2021

Date